The Pennsylvania State University

The Graduate School

College of Engineering

OPTIMIZATION OF POWER GENERATION IN AIRBORNE WIND ENERGY SYSTEMS

A Thesis in

Mechanical Engineering

by

Ramya Cheruvu

Submitted in Partial Fulfillment

of the Requirements

for the Degree of

Master of Science

May 2015

The thesis of Ramya Cheruvu was reviewed and approved* by the following:

Hosam Fathy
Assistant Professor of Mechanical Engineering
Thesis Advisor

Christopher Rahn
Professor of Mechanical Engineering

Karen A. Thole
Professor of Mechanical Engineering
Head of the Department of Mechanical Engineering

*Signatures are on file in the Graduate School

ABSTRACT

Optimization of power generation is important for Airborne Wind Energy Systems to increase their cost effectiveness and hence industry viability. In this thesis, an approach to optimal control of airborne wind turbine along with shape optimization of wind turbine is proposed. A simplified model of an airborne wind turbine, constrained for motion along the vertical direction is considered. The Panel method is used for analysis of flow field and pressure distribution on the airborne wind turbine. The results of this analysis are used to compute real-time lift forces acting on the turbine, which in turn give the power generated at each instant in time. An optimal strategy, using Dynamic Programming algorithm, has been developed to maximize the integral of instantaneous power generated, by adjustment of altitude and orientation of turbine.

TABLE OF CONTENTS

LIST OF FIGURES

ACKNOWLEDGEMENTS

I would like to thank my advisor Dr. Hosam Fathy for his relentless support, guidance and encouragement through my Master's program. I would also like to thank him for his time and effort in reviewing the thesis. The knowledge and experience I have gained from guidance is invaluable.

I would also like to express my thanks to my parents, brother and friends for their continuous support, patience and guidance.

Chapter 1

Introduction

1.1 Summary

This thesis examines the broad problem of optimizing the trajectory of an **airborne wind energy system (AWES)** to maximize its average output power. The thesis is motivated by three key factors. First, airborne wind energy systems are growing in popularity, thanks to their low cost, versatility, and ability to extract energy from high-speed wind at higher altitudes compared to conventional wind power systems. Second, airborne wind systems have more degrees of freedom that conventional wind turbines, thanks to the fact that they are attached to the ground through flexible tethers rather than rigid towers. The power they generate depends on their movement relative to the wind, and is therefore strongly path-dependent. This creates an opportunity for increasing airborne power generation significantly through trajectory optimization. Third, the power generated by an airborne wind energy system also depends on the aerodynamic design of the system, creating an opportunity for optimal aerodynamic shaping.

The literature presents control methods and optimization strategies for maximizing the power generated by a given AWES. Most of this work focuses on open- and closed-loop control for airborne wind systems with **ground-level power generation** [15]–[25], although there is growing interest in applying methods such as model-predictive control (MPC) to **airborne generators** (ABGs) [26, 27, 28]. The problem of simultaneously optimizing the shape and flight trajectory of an airborne wind energy system remains unaddressed by the literature, and is the focus of this thesis. Specifically, the thesis develops a framework that combines the **panel method** with **deterministic dynamic programming** to enable trajectory optimization for an

arbitrarily-shaped airborne wind energy system. While this framework has not been used for shape optimization in this thesis, the tools developed herein make shape optimization possible in conjunction with trajectory optimization for airborne wind energy systems.

1.2 Background and Motivation

Motivation for this thesis stems from the growing global energy needs and the costs of the fossil fuels needed to meet some of these needs, both from a financial and monetary perspective. Wind energy is an attractive renewable alternative to fossil fuels, and is abundant to the point where even if only 20% of global wind resources are exploited, they would provide 100% of global energy needs and 7 times the global need for electricity [1]. Wind energy has the additional advantages of being widely distributed, inexhaustible, and relatively clean with favorable greenhouse gas emissions (GHG) compared to fossils [2]. Investments in wind energy can be scaled to the meet the needs of local communities, and can grow as these needs grow (subject to constraints on land use). Thanks to these advantages, wind power production has grown at an average annual rate of 34% in the last five years and is the fastest growing source of electrical energy [3]. In June 2014, the total contribution of wind power to worldwide energy production was only 4%, but this percentage is likely to grow with time [4]. Significant efforts are being made to increase the cost competitiveness of wind power compared to fossil fuels, by improving the turbines used for harvesting wind energy and overcoming the limitations in conventional energy harvesting mechanisms. Airborne Wind Energy Systems (AWES) or tethered wind energy systems are being explored as next stage in the development of wind turbine technology to fully utilize high-altitude wind power [5]. Prototypes of possible AWES have been developed by various industries and research communities [7]-[13].

Conventional wind turbine harvests the kinetic energy of the wind using rotary components, which consist of blades that rotate in the wind, and drive train mechanisms that convert the low-speed rotational energy of blades into high-speed rotation suitable for electricity generation. A schematic of conventional wind turbine is shown in Figure 1.1. The rotor is mounted on a tower which usually contains a drive train, a generator, systems to point the rotor into the wind and other necessary mechanisms. In case of offshore wind turbines, the generator is located on land.

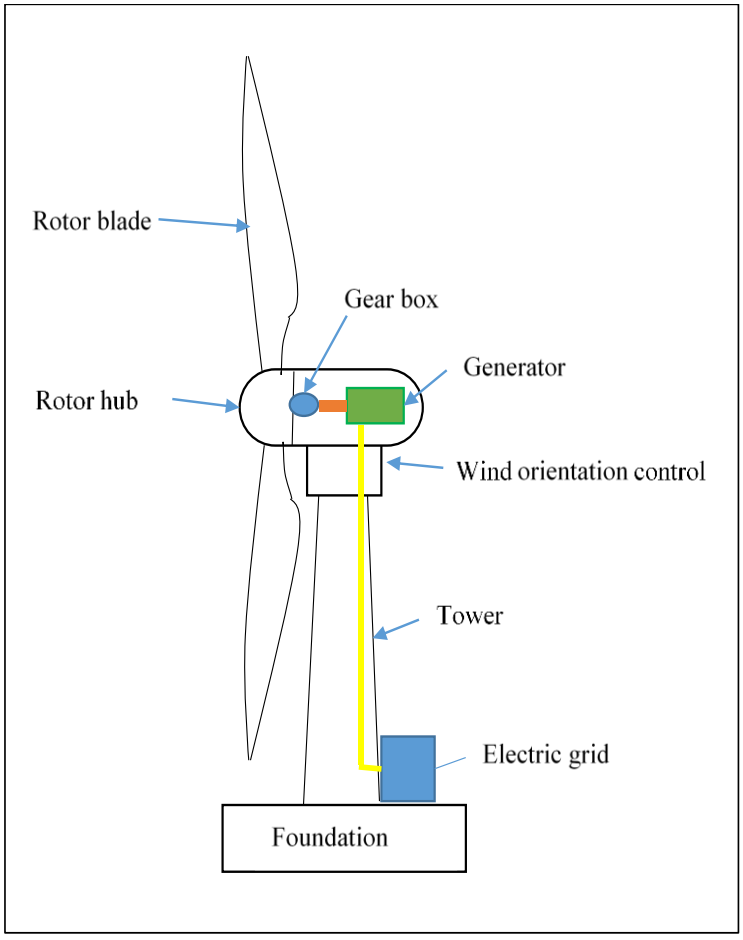

Figure **1-1**: Schematic of a conventional wind turbine

The scientific community has aggressively pushed for better conventional wind power systems, i.e., systems with higher power delivery capabilities, better reliability, and lower cost [5]. Efforts to achieve this include the optimal shaping of wind turbine blades, the refinement of turbine control systems, the optimization of the number of blades, and the efficient use of material to reduce the size and cost of wind turbines, thereby reducing the cost of electricity generation [5]. A particularly appealing opportunity, in this context, is the extraction of power from high-altitude wind. The power extracted by a wind turbine increases with wind speed cubed. That is, a 10% increase in the wind speed results in 33% increase in energy extracted by the turbine. Winds at higher altitudes have been found to have greater speeds with more persistence and less turbulence compared to winds at altitudes of 50-150 m from the ground, which is generally the operating range of conventional wind turbines [5]. The sizes and heights of wind turbines have grown to extract more energy from the surrounding wind and take advantage of the higher and persistent velocities of wind at higher altitudes [5]. Turbine installations have reached roughly 100m in diameter, with power production levels of 3-5MW per turbine [5]. However, the extraction of high-altitude wind power above 150m by further increases in size remains infeasible, as material and installation costs exceed the revenues from additional wind generation. Further increases in size also create significant structural design challenges. The airborne wind energy paradigm proposes elimination of structural elements such as towers not involved in power generation and replacing them with tethers and cables to support and enable the movement of an airborne rotor, as shown in Figure 1.2. Electrical or mechanical power, depending on location of generator, is transmitted to ground using cables.

The use of tethered wind energy systems in place of fixed tower installations allows for the following advantages. First, most of the energy produced by conventional wind turbines is harvested by the periphery of their blades. An AWES, in contrast, harvests wind energy using the entire body of the rotor operating over a wide swept area, thereby collecting more wind energy.

As such, the AWES can have a much larger effective span compared to a fixed system. Second, the operating altitude of AWES can be as high as 1000m, and can furthermore be adjusted to seek the altitudes at which wind speeds are highest at any given time. This provides an inexpensive solution for harvesting high-velocity wind energy.

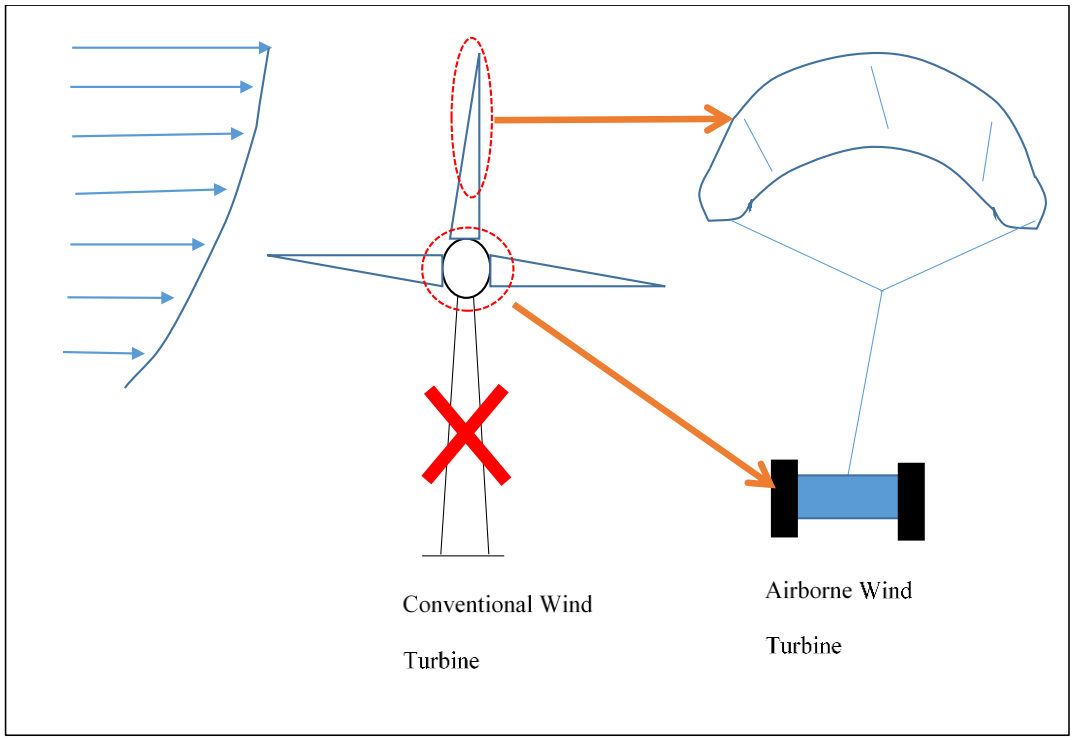

Figure **1-2**: Difference between conventional wind turbine and AWT

While the above advantages or airborne wind energy systems are attractive, these systems also have significant disadvantages and limitations. First, these systems need tethers and cable of sufficient strength to withstand the forces generated by high-speed AWES travel. This becomes particularly expensive at altitudes of 200m and above. Second, the rotor mass (with or without a generator), together with the associated tethers and cables moving through the air at great speeds, is a safety concern. Any damage to personnel and surroundings in case of accidents is likely to be much higher with airborne wind energy systems compared to stationary turbines, given their

higher speeds. Third, airborne wind turbines require more land space compared to conventional wind turbines. This problem is particularly acute in wind farms employing multiple airborne turbines: these turbines cannot be placed too close to one another, or else there is a risk of tether entanglement and severe damage. Fourth, special mechanisms and control algorithms are needed for launching some AWES systems to altitude. Failure of the launch mechanisms before or during takeoff can cause risk and damage to both hardware and personnel. Finally, operating airborne turbines at high altitudes and velocities is a complex control problem fraught with issues such as unmodeled dynamics (e.g., tether elasticity), increased susceptibility to weather conditions, and increased maintenance requirements.

The above safety concerns and space constraints make it important to maximize the power generated by a single airborne wind turbine, regardless of whether the turbine is used solo or as part of a multi-turbine system. To optimize AWES power generation, the trajectory of the rotor must be tailored to achieve maximum power. As explained later in the thesis, this often entails achieving a certain level of crosswind motion. Research and industrial organizations have been developing prototypes of various AWES configurations and are exploring several control and optimization algorithms to improve their performance. Some of the currently existing AWES configurations are discussed in the following section.

1.3 AWES configurations

There are multiple varieties of airborne wind energy systems, and multiple ways to classify them. For instance, one can classify these systems based on whether they are aerostatic or aerodynamic, whether they use ground-level or onboard generation, the material of the rotor, the number of tethers, and whether the rotors employ stationary or crosswind flight. This section

discusses these various classification criteria very briefly, focusing on the main advantages and disadvantages of each type of AWES.

Aerostatic vs. Aerodynamic Rotors

The rotor of an AWES can be aerodynamic (i.e., "heavier than air") or of the aerostat variety (i.e., "lighter than air"). Figure 1.3 illustrates these two types of rotors. Aerodynamic rotors such as kites and gliders (both soft and hard wing material) utilize wind lift to sustain their flight. In contrast, aerostatic airborne wind energy systems are supported in the air by buoyancy. Aerostatic systems have the advantage that they are able to launch into flight without needing a dedicated launch mechanism, and are furthermore able to sustain flight even in very low-wind conditions. However, a key disadvantage of aerostatic systems is that it is difficult to make an AWES lighter than air: expensive material is needed to construct the system, and this material must be inflated using a light gas (e.g., helium). This is particularly problematic given the possibility of helium gas leakage from aerostatic systems, and the associated need for maintenance and refilling.

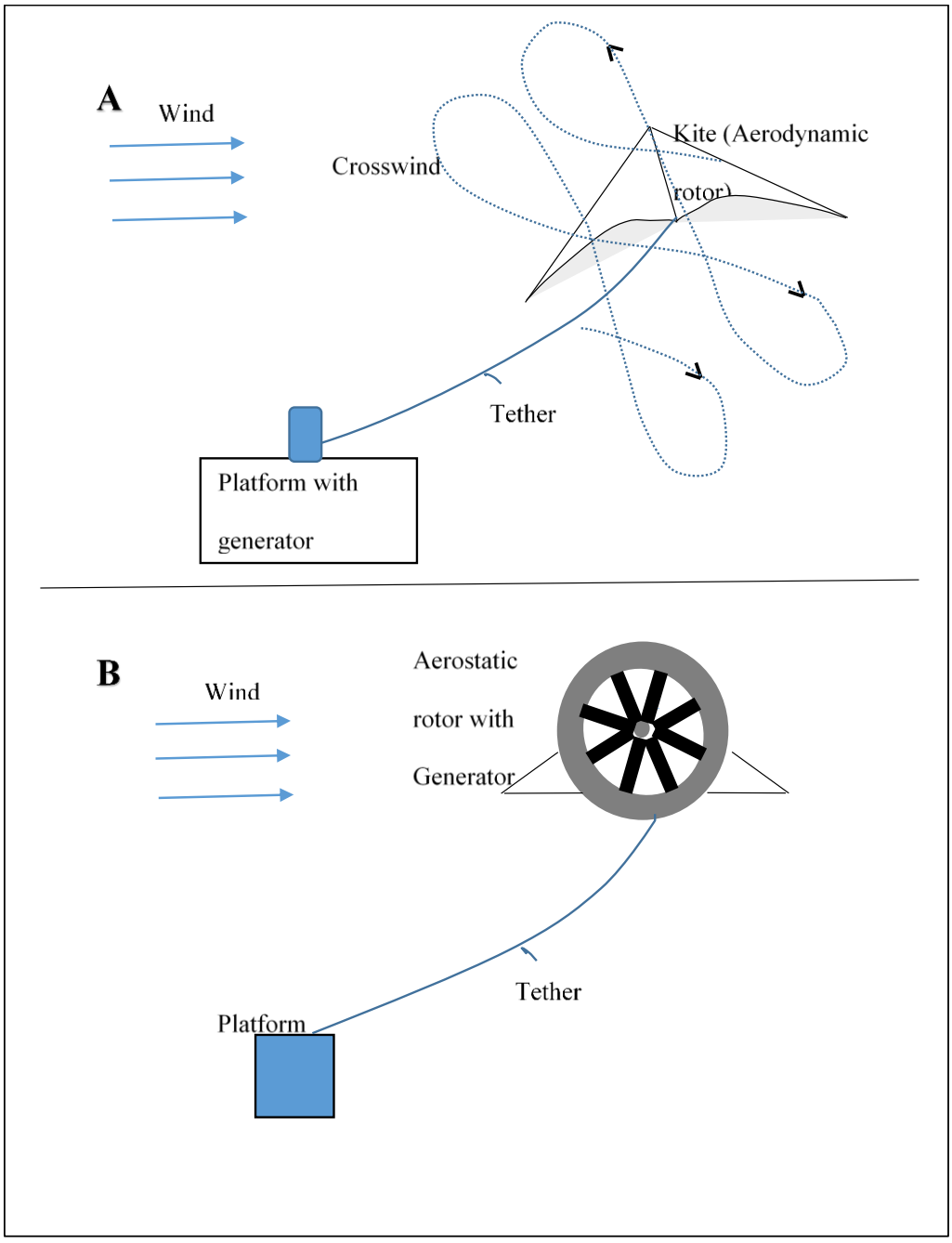

Figure **1-3**: Common schemes of AWES.

Airborne vs. Onboard Generation

AWES systems can be further classified based on the location of their electrical generators: some systems utilize onboard generation, while others use ground-level generation (GLG). In the former case, electricity must be transmitted to the ground, typically through electrified tethers. In the latter case, the tethers transmit mechanical energy to the ground, where it is converted to electricity.

AWES systems with ground-level generation, as in [7-9], typically operate in two phases: an extraction (generation) phase and a passive phase. The trajectories they follow are either similar to a yo-yo or carousel (i.e., a figure-8 orbit or a circular orbit) [19]. An example of the GLG configuration is shown in Figure 1.3A. Power is generated when the kite, connected to the generator by a cable, is reeled out. Conversely, power is consumed to reel the kite back in. Systems with onboard generators, such as the system in Figure 1.3B and [12], generate power continuously as seen in both the Makani and Altaeros commercial systems.

Both ground-level and onboard generation systems have their own technical advantages and different sets of compromises. On the one hand, ground-level generation systems are appealing because:

1. They are lightweight, more robust, and have simpler designs compared to onboard generation systems.
2. They are less likely to cause damage in case of accidents, thanks to the lower masses of their airborne components.
3. Mounting a generator on a flying rotor restricts the size of the generator that can be used: a constraint that does not exist in ground-level generation systems.
4. Greater loading means that the rotors and tethers or airborne systems are likely to experience higher mechanical stresses, and are therefore more vulnerable to mechanical failure compared to GLG systems.

5. Airborne systems require conductive tethers to transmit electricity, which can be costlier than the tethers needed for GLG systems (which only need to transmit mechanical energy).

On the other hand, there are also reasons why airborne systems can be appealing:

1. The fact that ground-level generators have two distinct operating phases – one where power is generated and one where it is used – can be challenging from an electrical systems perspective. For example, this fact may create a need for substantial ground-level energy storage and power conditioning equipment to smooth the two-phase power generation of a GLG system. This can drive up the overall levelized cost of the generated electricity [14].
2. A further disadvantage of ground-level generation is the fact that it forces the airborne wind system to follow a certain family of trajectories (i.e., two-phase trajectories). This is a constraint that could make it difficult to optimize power generation by, say, always flying at the altitude where wind speed is maximum.
3. The trajectory of a GLG system has to be optimized for power generated to be greater than power consumed during the passive phase. In contrast, airborne systems often do not require trajectory optimization to generate positive power. In particular, they are often capable of producing positive power during non-optimized stationary flight (although there remains a possibility that trajectory optimization will produce even more power).

Other Classification Criteria

Additionally, AWES systems can be categorized based on material of the rotor, number of tethers, crosswind flight or stationary flight etc. Rotors can be made of soft material, hard material or they can be lighter-than-air. Models with soft kites tear easily, operate at low

velocities and require frequent maintenance and replacement whereas hard winged kites though resilient and give higher velocities, are more of a safety hazard in case of accidents. Lighter-than-air systems are usually more expensive as they require gases such as helium, but they support the rotor in air even in the absence of velocity gradients [14].

Single-tether AWES systems are generally less safe because damage to the tether can bring down the entire system, but they have the advantage of lower tether drag and hence reduced losses. Multi-tether systems have more losses, both due to the multiplicity of the tethers and the friction losses at the winches, but their redundancy does provide additional safety in case of tether failure [14].

Crosswind flight of the rotor generates more power compared to a stationary rotor due to increased apparent velocity. However, crosswind flight requires a large unused airspace, has tether drag, and poses risk to personnel operating the turbine because the high speeds associated with crosswind motion reduce tether visibility. Crosswind systems have the potential to cause much more damage than stationary rotors in case of operational failure. Crosswind flight also requires complex control systems to follow an efficient trajectory [14].

The tradeoffs between the above types of airborne wind energy systems are non-trivial, and therefore no single system can be deemed “best”. Perhaps this is reflected in the sheer variety of such systems being explored for commercial applications. The airborne wind turbine developed by Makani uses a hard-winged kite that flies aerodynamically and carries an onboard generator. The generator is connected to the ground through electrified tethers, and is used both for onboard power generation and system launch. The Ampyx airborne power generator employs a glider tethered to a ground generator. KiteGen and Skysails have explored the use of soft kites to drive ground and offshore generators, respectively. Finally, Altaeros has been exploring the use of a tethered helium-filled shroud to lift an onboard turbine into the air.

1.4 Goals and Approach

The main goal of current work is to optimize the power generation of an AWT to increase their reliability and industrial viability. Majority of work in the literature is focused on performance improvement by optimization of figure eight or circular trajectories for GLG systems. Several control approaches and optimization algorithms developed for closed loop control and to handle issues, due to non-linearity, instabilities and environmental uncertainties encountered in efficient operation of GLG systems, are briefly discussed in Chapter 2. Work on control and optimization strategies for ABG systems is comprised of development of relaxation strategy, by Zanon and Diehl, for easy solution of general optimization strategy applicable to all types of AWES, and Model Predictive Control approach for stationary and altitude flight control by Vermillion *et al*. This thesis explores the application of Deterministic Dynamic Programming algorithm to improve performance for these systems. DDP is used to develop a control and optimization strategy for maximization of power generation in AWES, by utilizing system feedback and extrapolated information about the surroundings from wind velocity.

In order to achieve this goal, the following approach has been taken. A simplified model of the turbine with one degree of freedom is used. The analysis of forces and pressures acting on the turbine due interaction with fluid (air) has been considered. The Panel method was used to analyze the parameters of rotor environment, and it has been programmed for comprehensive flow field analysis, to include velocity and pressure distribution, lift force, pitching moment and profile drag acting on the airfoil. Use of Panel method for analysis gives this thesis flexibility in shape of the rotor and turbine model. The results of this analysis have then been exploited to calculate forces acting on the simplified system model and design an optimal control strategy for

altitude control and power maximization. DDP algorithm ensures optimal trajectory of the turbine through control of position and orientation of the rotor.

Chapter 2

Literature review

The previous chapter briefly introduces the concept of airborne wind energy, and presents examples of systems that harvest this energy, along with their relative advantages and disadvantages. This chapter provides a deeper presentation of the airborne wind energy literature, focusing on the use of optimization and control to maximize airborne power generation.

The use of airborne wind generation systems fundamentally builds on the premise that the flight of an aerodynamically efficient rotor through high-velocity wind induces enough lift and drag force magnitudes to ensure positive overall power production (and in certain cases support the flight of the rotor). To the best of the author's knowledge, the first rigorous analysis supporting the feasibility of power production using airborne wind generators appears in Miles Loyd's seminal paper, *"Crosswind Kite Power"* [4]. This paper shows that a single-unit airborne wind turbine (AWT), with an aerodynamic kite as the rotor, can produce 45MW of power. This represents a significant improvement in power generation compared to conventional wind turbines of the same size. Loyd argues, in fact, that airborne wind systems can potentially produce as much as 3-20 times the power of conventional turbines of the same size [4].

Loyd's paper examines a kite restrained by tethers, and uses a dynamic model of a C-5A aircraft to simulate this kite. There are at least two ways in which this kite can be used for airborne wind power generation: the kite can be held stationary by the tethers at high altitudes, or it can fly in crosswind patterns. During crosswind flight, either lift or drag can be used as a mechanism for power generation. Loyd's paper shows that the amount of power generated during crosswind flight is comparable regardless of whether lift or drag is used for power generation. More importantly, the power generation capacity in crosswind flight is related to

stationary power generation capacity by the multiplicative factor $\frac{(\frac{L}{D})^2}{2}$, where L and D are lift and drag forces, respectively [4].

The above finding by Loyd is very significant: it implies that crosswind power generation capacity exceeds stationary power generation capacity by a factor related to the square of lift-to-drag ratio. Crosswind flight is therefore quite advantageous, especially if lift-to-drag ratios of 6-7 are achieved. This result can be explained physically as follows: in a stationary generator, power is produced because of the wind forces acting on the generator's turbine blades, and is proportional to wind speed cubed. In contrast, crosswind power is a function of the apparent wind speed seen by the airborne wind energy system, and is proportional to the cube of this apparent speed. Flying crosswind at high velocities results in a large apparent wind speed vector, thereby increasing power generation substantially [4].

To achieve the power generation levels predicted by Loyd's feasibility analysis, one must carefully optimize both the *design* and *control* of a given airborne wind power system. Important design factors include kite sizing, kite and tether strength-to-weight ratios, landing and launch mechanism design, power transmission design, etc. The effect of launching mechanisms, transmission modes and tradeoff between efficiency and strength-to-weight ratio has been explored in [35, 36, 37, and 38]. The studies in the literature involving optimal rotor design and configuration have been restricted to comparing the advantages of dual airfoil over single airfoil wind turbines [22]. Detailed design factor studies such as these are important, but do not address the broader need for a system-level experimental validation of airborne wind power.

To the best of the author's knowledge, the first successful experimental demonstration of airborne power generation was realized by Canale *et al.* at Politecnico Di Torino in their study on a small-scale prototype named KiteGen. KiteGen consists of a tethered airfoil driving a generator on the ground. In other words, it is a ground-level generation (GLG) system. KiteGen's control

system was designed by Canale *et al.* to achieve two distinct flight phases [17, 18]. The kite generates energy during its *traction phase* and once maximum tether length is reached, the kite is reeled in during *recovery phase* to begin a new cycle. Considering the nonlinear, open-loop unstable nature of the kite model with relatively fast dynamics, Canale *et al.* applied model-predictive control (MPC) to a kite simulation model, with periodic boundary conditions. The controller's goal is to maximize the power generated during the traction phase (force x velocity) and minimize power consumed during the recovery phase. Since the time taken for solving this optimization problem was found to be 0.45s, the optimal control inputs were computed offline for a set of samples and approximated in real time. The simulation results showed 75 figure-8 shaped orbits in traction phase with power generation of 1.58 KW [17]. Also, the velocity of the kite is found to be 15 times greater than the rotor's tangential speed. This higher effective wind speed seen in KiteGen gives it a significant advantage over conventional wind turbines.

One important advantage of a combined simulation/experimental study is that it can provide insight into the *scalability* of the proposed wind power technology. Canale *et al.*'s simulation studies, for example, exhibit good agreement with experiments in terms of the predicted power generation level [18]. This is true for both the yo-yo configuration (where figure-8 flight is used) and carousel configuration (where the orbits are circular) [18]. Building on these results, Canale *et al.* conjecture that 100 kites, each of 500m^2 area and a lift-to-drag ratio of 12, flying in wind of 12m/s nominal speed and attached to a 1500m-radius carousel can generate 1000MW of power with land occupation of 7-8km^2. Canale *et al.* estimate that such a system would have an energy production cost ten time slower than that of a thermal plant of the same capacity. Furthermore, they emphasize the fact that a conventional wind farm area of up to 300km^2 and a cost 50% higher than comparable fossil fuel plants would be necessary to generate the same levels of power [18]. While these analyses and conjectures are very encouraging, one must take them with a grain of salt: only 11 of the proposed kites are needed to cover the area of

an entire football field, and the full KiteGen carousel system (sketched in Figure X below) would consume roughly 60-70% of the area of State College, Pennsylvania.

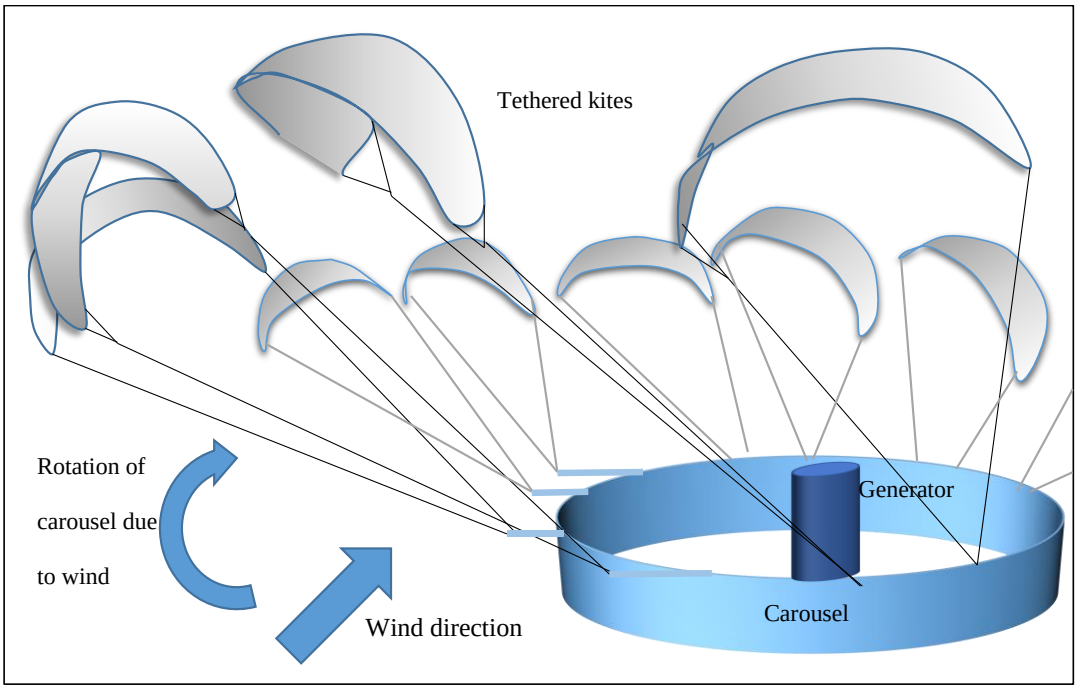

Figure **2-1**: KiteGen Carousel

The power generated by an airborne wind system is highly trajectory-dependent: flight trajectories that are capable of maintaining high crosswind velocities for substantial periods of time, for instance, are likely to generate more power. Much of the literature on trajectory optimization for airborne wind power generation builds on the pioneering work of Houska and Diehl [15,16]. Houska and Diehl applied a periodic optimal control strategy to a GLG system and solved the optimization problem for the objective of maximizing average power at the generator using a direct multiple shooting algorithm. Their work used a kite model from the literature, similar to the KiteGen model, and they optimized power generation by varying lift and drag coefficients during different flight phases. Specifically, their algorithm was designed to

achieve minimal lift during the recovery phase and maximum lift during the generation phase [15, 16]. They applied this method to single- and multiple-kite systems and showed power generation levels of 5MW (with a single kite) and 14.86MW (with double kites each of are $500m^2$), respectively. The trajectories optimized by Houska and Diehl are open-loop unstable, and require online feedback control if they are to be followed accurately in a real physical system.

The above research by both Canale *et al.* and Houska and Diehl [15-18] reveals an important fundamental conclusion about airborne wind energy generation: the optimal flight trajectory for airborne wind power is consistently either a figure-8 trajectory (for yo-yo systems) or a circular trajectory (for carousel systems). While these conclusions are important, three critical research challenges need to be addresses before they become practically implementable. First, there is a need for examining the **complex tradeoffs** involved in airborne flight trajectory optimization. Power maximization is important, for instance, but how does it affect tether tension? Are the resulting tether forces going to be excessive, to the point of potentially inducing damage? Is this a tradeoff that can – or should – be addressed using multi-objective Pareto optimization? Second, there is a need for optimization algorithms that are **sufficiently tractable** to enable real-time implementation in an airborne system. This is particularly true if there are modeling uncertainties that necessitate real-time, online optimal control. Third, there is a need for exploiting the inherent **time-scale separation** between trajectory optimization and servo control in airborne wind power systems. Given the number of degrees of freedom of an airborne system, it is not expedient to optimize all flight parameters simultaneously. Perhaps some of these parameters can be used to meet servo control needs such as flight stabilization. The remainder of this literature review addresses each of these needs in more depth.

Multi-Objective Optimization in Airborne Flight

Landsorp *et al.* generated complex trajectories for optimal power generation by solving a periodic optimal control problem to minimize the weighted cost function selected to give maximum average power per cycle [19].

Computational Tractability for Real-Time Implementation

Zgraggen *et al.* developed an optimization algorithm that can be applied in real time to optimize the trajectory. This algorithm has been designed so that it can be applied to any model or can be used as an extension to an existing control system. The algorithm uses location of the airfoil with respect to altitude and wind direction and optimizes force acting on tether as a result, instead of optimizing shape of the trajectory. This eliminates the issue of sub-optimal trajectories in real time when using offline solutions and removes computational time of NMPC approach. The authors have proved the efficiency of this approach with both simulation and experimental results. The effects of turbulent wind and uncertain sensor readings are also eliminated [20].

Gros *et al*. have explored several approaches to deal with the nonlinear process dynamics of the airborne wind system and also overcome drawbacks in NMPC approach. They explored relaxing the constraints of optimization problem, by removing feedback loops to reduce nonlinearities and couplings in the model of AWES system, which allows for use of Newton-type optimization techniques with good initial guesses and later applying homotopy strategy for extending the solution to nonlinear problem. The optimization problem was applied for both circular and figure 8 trajectories. The resultant power generation was not high due to absence of optimized wing model and a single orbit per pumping cycle. This increases the performance of NLP solver in computing optimal power trajectory [21]. Gros *et al*. have explored the use of a

fast NMPC scheme based on Real-Time Iteration to track a reference trajectory under the assumption that pitch-yaw-roll of the kite model are tracked by a separate inner controller. This assumption reduced the computation time of NMPC controller making it suitable for real time application. The RTI scheme is used to reduce computation time and control update latency issues in NMPC. It has been designed to perform a single Newton-type iteration instead of several SQP steps per input update and also computes input update without prior knowledge of process state greatly reducing computation time. It is also assumed that complete knowledge of the process states are available [22]. They have extended this further by including Moving Horizon Estimator observer to estimate wind turbulences in the previous fast NMPC scheme and pitch-yaw-roll control is also handled directly by NMPC. The time for NMPC and MHE computation was found to be well within sampling time period with margin, improving scope for real time trajectory optimization [23]. They have further applied this strategy to dual configuration airfoil and compared efficiencies of single and dual airfoil configurations where the additional challenge of stabilizing the system is met by using direct multiple shooting method for optimization. The cost function was found to be sub-optimal in terms of energy production which leaves scope for selection of cost functions that result in maximum energy production [24].

Costello *et al*. present a dynamic model of kite suitable for dynamic optimization and proposed RTO ("Real Time optimization") scheme to achieve optimal trajectory using parameter estimation and model-based optimization till controller converges to an optimal trajectory. The resulting scheme was applied to simulation of kite and boat system, and RTO has been shown to reduce the effect of instabilities due to modeling mismatches and disturbances [34].

Hierarchical Control in Airborne Wind Energy Systems

Zgraggen *et al.*designed a control strategy for simplified model with an outer loop control to compute desired reference heading and inner loop control to achieve reference heading. These control strategies have advantage over constrained optimal and NMPC solutions in that they need not solve complex non-linear solutions and can be actually applied in real time and are useful for experimental work. However, these strategies do not always track globally optimal trajectories needed for maximum energy production for that airborne wind system which is critical for tethered airfoils [25].

The recent work by Vermillion *et al* has been focused on *formulation of optimization algorithm* for ABG systems, with use of NMPC controllers for *Hierarchical control* [26, 27, and 28]. These specific optimization and control algorithms are designed to take advantage of continuous power generation phase of ABG systems which enables for altitude and crosswind optimization. Vermilion *et al.* have developed a hierarchical control structure for model predictive stationary downwind flight control, longitudinal flight control and altitude and crosswind motion control for a prototype of Altaeros lighter-than-air wind turbine [26-28]. The closed loop MPC control system in [28] is developed for both altitude and crosswind control, where closed control law is used for crosswind flight control and MPC is only used for altitude optimization which removes computational complexity associated with NMPC. Also, the algorithm has been designed track optimal operating point of the turbine and enable optimal performance by constraining the altitude and crosswind velocity to produce that rated wind speed which results in maximum efficiency of the turbine. These papers provide prospective avenue for development of trajectory optimization methods designed for characteristic advantages of ABG systems.

In conclusion, there is a rich literature on airborne wind energy system design and optimization. The literature shows the feasibility of airborne wind energy systems, and highlights

the value of fast cross-wind flight in such systems. Two particular trajectories are seen as optimal by the literature: the figure-8 flight trajectory for yo-yo systems, and the circular trajectory for carousel systems. To implement these trajectories in a practical setting, there is a need for computationally efficient online optimization, perhaps in conjunction with hierarchical control. A rich literature exists addressing these challenges. However, there are open gaps in this literature, and important challenges that remain unaddressed. In particular, the link between kite design optimization and control trajectory optimization remains relatively unexplored in the literature. It is this fairly unexplored link that justifies the research presented in this thesis. In particular, the thesis focuses on computing a globally optimal trajectory using deterministic dynamic programming for a simplified airfoil/rotor model. The motion of the rotor is constrained to one dimension: a fact that reduces the problem to altitude trajectory optimization. This thesis differs from previous optimization strategies by incorporating information from the analysis of rotor and environment by using the Panel method. This enables the practitioner to compute and analyze the effect of shape/structure of the rotor on the performance, thereby allowing for comparison and design of an aerodynamically optimal rotor before constructing a prototype.

Chapter 3

AWES Airfoil Analysis Using the Panel Method

This chapter briefly describes both the panel method and its application for the determination of AWES airfoil drag and lift coefficients. The panel method is a technique for solving flow over 2D and/or 3D geometries, to calculate fluid velocity, and in turn pressure distribution on an object by replacing the object's geometry with singularity panels [29]. Using this technique, velocity distributions around the turbine of an AWES can be analyzed. The lift force acting on the turbine due to the surrounding fluid (air) is calculated by integrating pressure due to air over the turbine.

The panel method is predicated on the assumption that flow around the system is ideal (inviscid, irrotational and incompressible). Since the flow is ideal, velocity can be expressed as gradient of a scalar *potential function* [29], as shown below.

$$\vec{V} = \boldsymbol{\nabla\varphi} \quad (3.1)$$

where $\varphi = \varphi(x, y, z, t)$ is the potential function. For incompressible flow, the divergence of the velocity vector must be zero, i.e.

$$\nabla.\vec{V} = 0 \quad (3.2)$$

Combining the above two results gives the standard Laplace equation for the potential function, namely,

$$\nabla^2\varphi = 0 \quad (3.3)$$

Ideal flows are solutions to the Laplace equation. Linearity of this equation makes it possible to express solutions of the Laplace equation as weighted sums of specific ideal flow

patterns, as illustrated in Figure 3.1 below. This, in turn, makes it easy to solve for complex flow patterns under different boundary conditions.

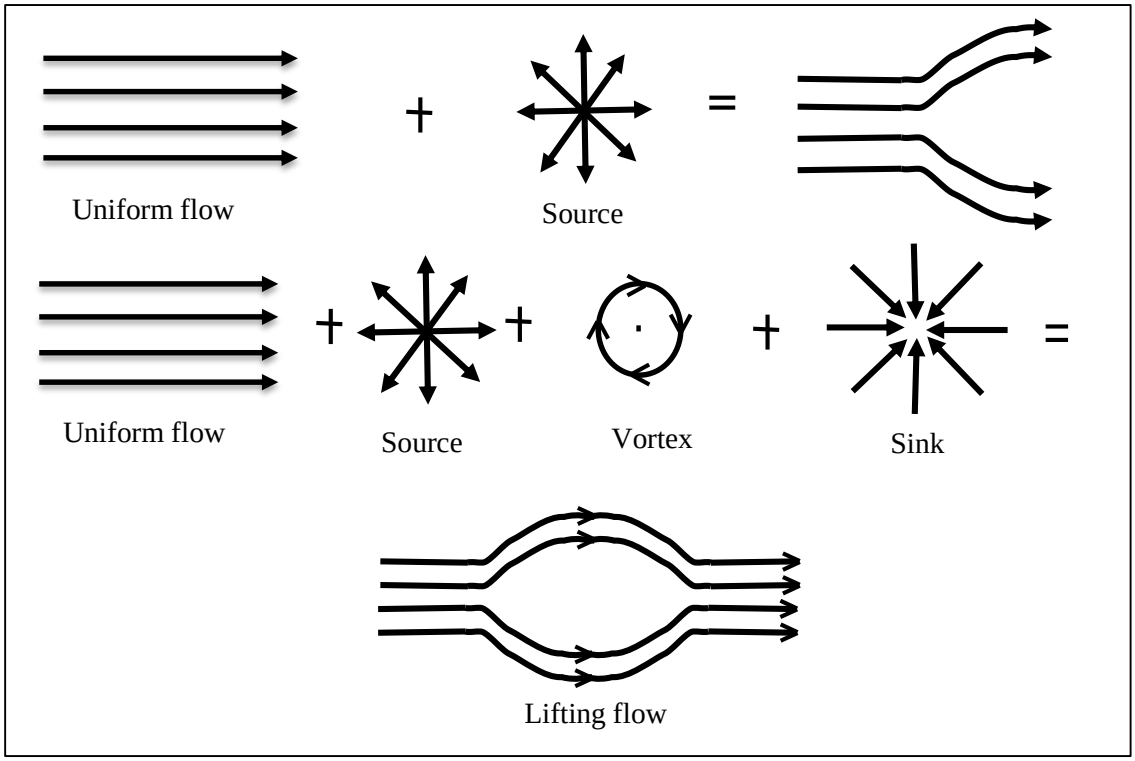

Figure **3-1**: Complex flow produced from elementary flows

The panel method finds the solution to a complex flow by starting with simple, elementary flows and adding them together to visualize complex patterns. The combination of flows which best describes the system in question is to be determined. For our purpose, i.e., flow of air over an airfoil geometry, the sum of uniform flows and series of sources, (called *source sheets*), represent the problem accurately [29]. The potential function of a source flow is given by

$$\varphi = \frac{Q}{2\pi} * lnr \quad (3.4)$$

where Q is source strength. A source sheet formed by a series of sources of infinitesimal strength Qds, will have infinitesimal potential over an infinitesimal length ds as shown below

$$d\boldsymbol{\varphi} = \frac{Qds}{2\Pi} * lnr \quad (3.5)$$

Furthermore, the total potential on the panel length ds is given by $\varphi(x,y) = \int_a^b \frac{Qds}{2\Pi} * lnr$ (3.6).

Source sheets are arranged to form a closed polygon shape that approximates the airfoil shape as closely as possible. Each panel is defined by two endpoints plus one control point (midpoint).

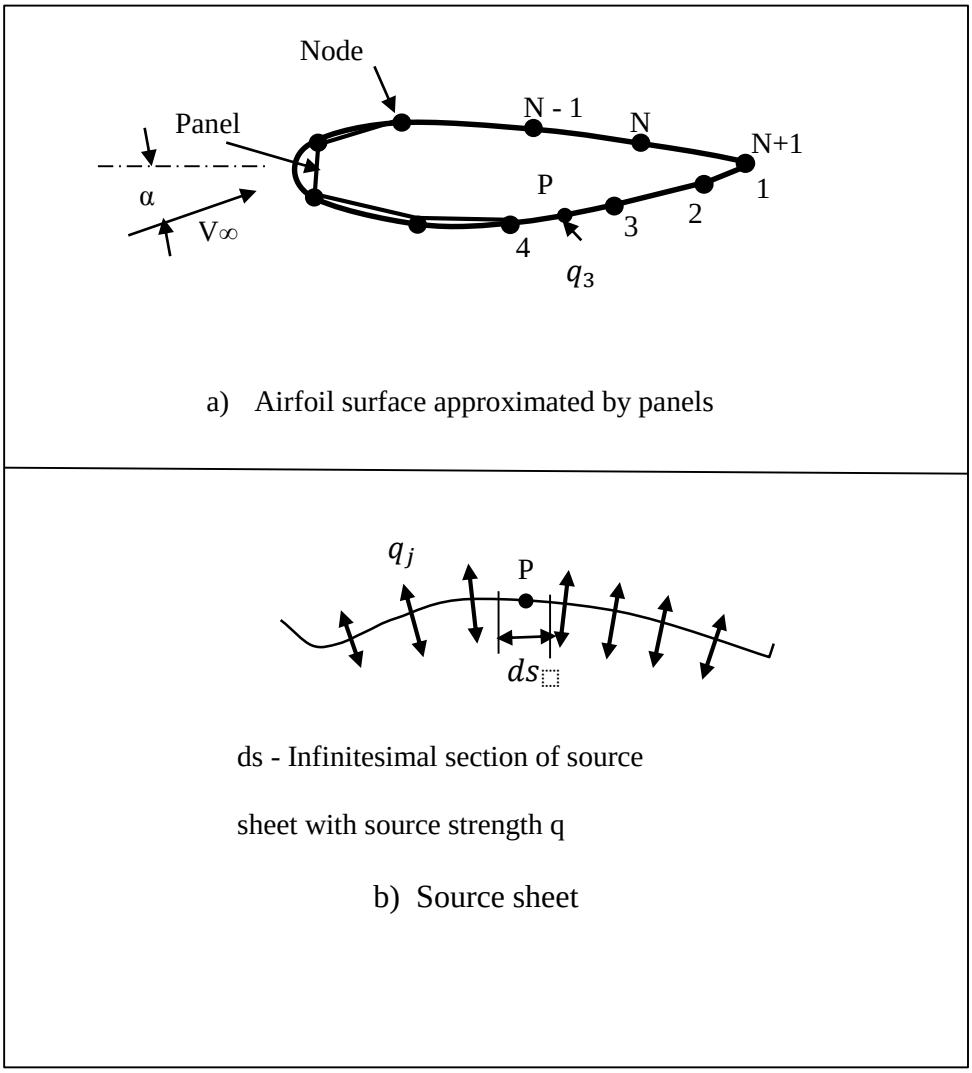

a) Airfoil surface approximated by panels

b) Source sheet

Figure **3-2**: A) Surface of airfoil approximated by panels. B) Source sheet

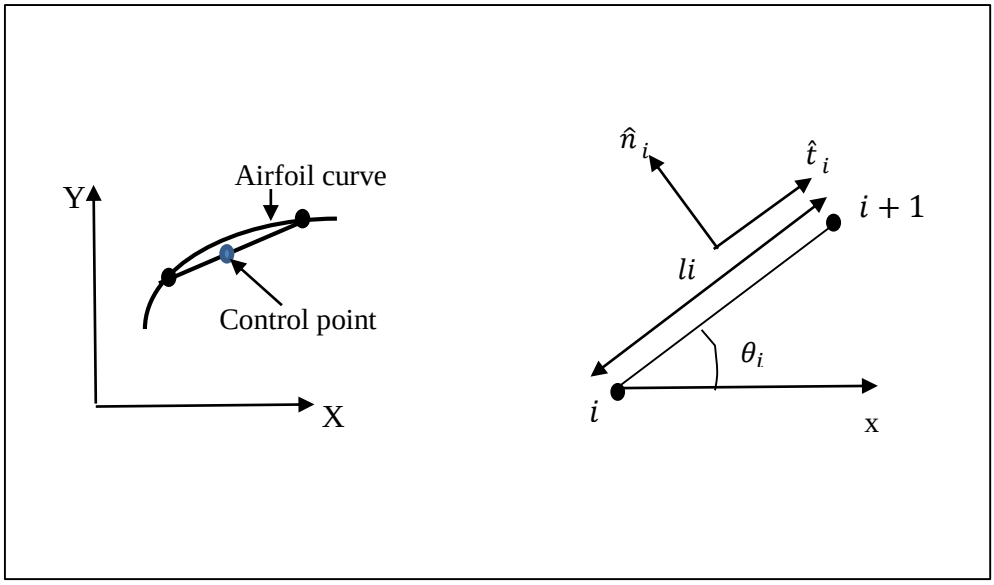

Figure **3-3**: Panel nomenclature.

Each panel is considered to produce a source flow whose strength is constant along its length. From Figure 3-2, we have N panels around the object. Therefore, N strengths have to be specified, one on each panel such that flow over the panels will be a realistic representation of flow over solid surface. This can be achieved by the non-penetration boundary condition which ensures that there is no flow through the surface of the airfoil by equating the component of velocity perpendicular to airfoil to zero. The end result is the following boundary condition:

$$\overrightarrow{V}.\hat{n}_i = 0 \quad (3.7)$$

The potential at a point P on the j^{th} panel due to a source at its control point is given by:

$$\varphi_j(x,y) = \int_j \frac{q_j ds_j}{2\Pi} * lnr_j \quad (3.8)$$

Since q_j is taken as constant across the panel, the above equation can be simplified to:

$$\varphi_j(x,y) = q_j \int_j \frac{lnr_j ds_j}{2\Pi} \quad (3.9)$$

The total potential induced at a point P on j^{th} panel due to sum of all infinitesimal sources is then given by the following summation,

$$\varphi_j(x,y) = \sum_{j=1}^{N} q_j \int_j \frac{lnr_{ij} ds_j}{2\Pi} \quad (3.10)$$

If the location of p is considered to the same as the control point of the panel, then r_{ij} equals the distance between P and the panels j = 1 to N. The term $\int_j \frac{lnr_{ij} ds_j}{2\Pi}$ represents the contribution of all panels to potential at P. Sources cannot replicate rotational moments acting on the airfoils. Therefore, point vortices have been added to the control points to simulate a lifting flow. Therefore, we now have *N sources* and N vortices (of same strength γ) at the control points on the panel. Equation (3.7) becomes

$$\varphi_j(x,y) = \sum_{j=1}^{N} \int_j \frac{(q_j lnr_{ij} - \gamma)}{2\Pi} ds_j \quad (3.11)$$

This gives an additional boundary condition, called the *Kutta condition*, which ensures that flow leaves the trailing edge smoothly. This condition is satisfied by equating the tangential velocity components of the top and bottom panels on the trailing edge assuming they are of equal length, leading to the following boundary condition:

$$\vec{V}.\hat{t}_1 = -\vec{V}.\hat{t}_N \quad (3.12)$$

The potential function for the onset uniform flow before the airfoil is

$$\varphi_\infty(x,y) = V_\infty x cos\alpha + V_\infty y sin\alpha \quad (3.13)$$

The resulting expression for potential through the flow field is given by sum of equations (3.11) and (3.13) due to principle of superposition.

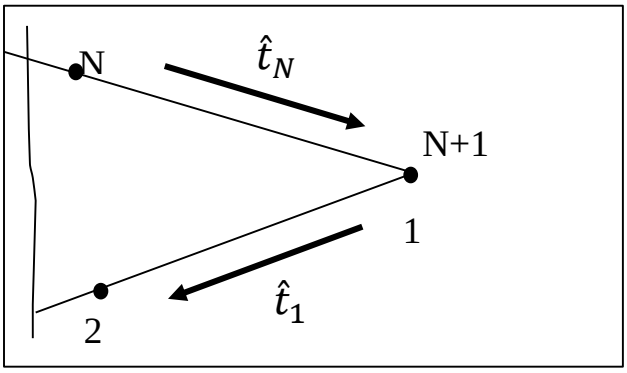

Figure **3-4**: Trailing edge.

$$\varphi \quad = \varphi_j + \varphi_\infty \quad (3.14)$$

Defining nomenclature on each panel, i^{th} panel with length l_i and inclination θ_i with respect to x-axis, lies between i^{th} and $i+1^{th}$ nodes are used to define equations (3.15)-(3.17).

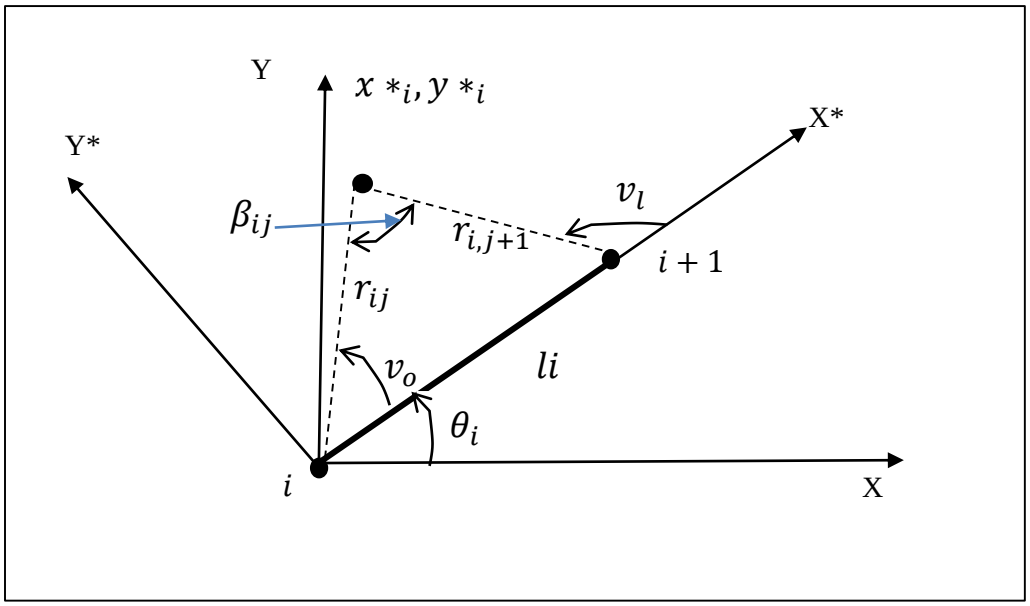

Figure **3-5**: Terms and coordinate system of the panel.

$$sin\theta_i = \frac{y_{i+1} - y_i}{l_i}, cos\theta_i = \frac{x_{i+1} - x_i}{l_i} \quad (3.15)$$

$$\hat{n}_i = -sin\theta_i \hat{\imath} + cos\theta_i \hat{\jmath} \quad (3.16)$$

$$\hat{t}_i = cos\theta_i \hat{\imath} + sin\theta_i \hat{\jmath} \quad (3.17)$$

For the velocity vector $\vec{V} = u_i\hat{\imath} + v_i\hat{\jmath}$, writing the boundary conditions (3.7) and (3.12) using above relations, for each i = 1…N

$$-u_i sin\theta_i + v_i cos\theta_i = 0 \quad (3.18)$$

$$-u_1 cos\theta_1 + v_1 sin\theta_1 = -u_N cos\theta_N + v_N sin\theta_N \quad (3.19)$$

Expressing velocities at each panel in terms of source and vortex distributions from equations (3.11), (3.13) & (3.14),

$$\varphi = V_\infty x cos\alpha + V_\infty y sin\alpha + \sum_{j=1}^{N} \int_j \frac{(q_j ln r_{ij} - \gamma)}{2\Pi} ds_j \quad (3.20)$$

$$u_i = V_\infty cos\alpha + \sum_{j=1}^{N} q_j u_{sij} + \gamma \sum_{j=1}^{N} u_{vij} \quad (3.21)$$

$$v_i = V_\infty sin\alpha + \sum_{j=1}^{N} q_j v_{sij} + \gamma \sum_{j=1}^{N} v_{vij} \quad (3.22)$$

where u_{sij}, u_{vij}, v_{sij} and v_{vij} are *influence coefficients* that indicate how force at a particular point influences force at other point due to geometry of the airfoil. Influence coefficients are first calculated in the local coordinate system aligned with the panel and converted to global coordinate system seen in Figure 3.5.

If u^* and v^* are influence coefficients in the local coordinate system, they can be transformed to global coordinate system by,

$$u = u^* cos\theta_j - v^* sin\theta_j, \qquad v = u^* sin\theta_j + v^* cos\theta_j \quad (3.23)$$

Influence coefficients at a point x^*, y^* due to source singularity q_j on panel j are given by

$$u^*_{sij} = -\frac{1}{2\pi}\ln\left(\frac{r_{i,j+1}}{r_{ij}}\right) \quad (3.24)[29]$$

$$v^*_{sij} = \frac{v_l - v_0}{2\pi} = \frac{\beta_{ij}}{2\pi} \quad (3.25)[29]$$

Influence coefficients due presence of vortex singularity on panel j are,

$$u^*_{vij} = \frac{\beta_{ij}}{2\pi} \quad (3.26)[29]$$

$$v^*_{vij} = \frac{1}{2\pi}\ln\left(\frac{r_{i,j+1}}{r_{ij}}\right) \quad (3.27)[29]$$

where r_{ij} is the distance from j^{th} node to point x^*, y^* and β_{ij} is the angle subtended at the same point by j^{th} panel as seen in Figure 3.5.

Now, we rewrite the equations as set of N+1 linear algebraic equation with N+1 unknown variables, by substituting equations (3.15 – 3.17) & (3.21 - 3.27) in simplified boundary conditions (3.18 – 3.19), to solve for source and vortex strength. After substituting the equation for velocity components and transformed influence coefficients in equation (3.18), we get a matrix of N equations,

$$\sum_{j=1}^{N} A_{ij}q_j + A_{i,N+1}\gamma = b_i \quad i = 1, \dots N \quad (3.28)[29]$$

where

$$A_{ij} = \frac{1}{2\pi}\sin(\theta_i - \theta_j)\ln\left(\frac{r_{i,j+1}}{r_{ij}}\right) + \frac{1}{2\pi}\cos(\theta_i - \theta_j)\beta_{ij} \quad (3.29)$$

$$A_{i,N+1} = \frac{1}{2\pi}\sum_{j=1}^{N}\left\{\cos(\theta_i - \theta_j)\ln\left(\frac{r_{i,j+1}}{r_{ij}}\right) - \sin(\theta_i - \theta_j)\beta_{ij}\right\} \quad (3.30)$$

$$b_i = V_\infty \sin(\theta_i - \alpha) \quad (3.31)$$

Substitution and simplification of Kutta condition (3.19) gives the N+1 equation of form

$$\sum_{j=1}^{N} A_{N+1,j} q_j + A_{N+1,N+1}\gamma = b_{N+1} \quad (3.32)$$

where

$$A_{N+1,j} = \frac{1}{2\pi}\left[\sin(\theta_1 - \theta_j)\,\beta_{1,j} + \sin(\theta_N - \theta_j)\,\beta_{N,j} - \cos(\theta_1 - \theta_j)\ln\left(\frac{r_{1,j+1}}{r_{1,j}}\right)\right.$$

$$\left. - \cos(\theta_N - \theta_j)\ln\left(\frac{r_{N,j+1}}{r_{N,j}}\right)\right] \ldots\ldots (3.33)$$

$$A_{N+1,N+1} = \frac{1}{2\pi}\sum_{j=1}^{N}\left[\sin(\theta_1 - \theta_j)\ln\left(\frac{r_{1,j+1}}{r_{1,j}}\right) + \sin(\theta_N - \theta_j)\ln\left(\frac{r_{N,j+1}}{r_{N,j}}\right) + \cos(\theta_1 - \theta_j)\beta_{1,j}\right.$$

$$\left. + \cos(\theta_N - \theta_j)\,\beta_{N,j}\right] \quad (3.34)$$

$$b_{N+1} = -V_\infty \cos(\theta_1 - \alpha) - V_\infty \cos(\theta_N - \alpha) \quad (3.34)$$

The derivation has been coded in MATLAB and solution the system of equations (3.28) - (3.32) gives the values of $q_{1\ldots N}$ and γ.

The source and vortex strength hence computed are used to calculate tangential velocity vector in the flow field which is given by,

$$u_{ti} = u_i cos\theta_i + v_i sin\theta_i \quad (3.35)$$

This equation after substitution yields

$$u_{ti} = V_\infty \cos(\theta_i - \alpha) + \sum_{j=1}^{N}\frac{q_j}{2\pi}\left[\sin(\theta_i - \theta_j)\,\beta_{ij} - \cos(\theta_i - \theta_j)\ln\left(\frac{r_{i,j+1}}{r_{i,j}}\right)\right]$$

$$+ \frac{\gamma}{2\pi}\sum_{j=1}^{N}\left[\sin(\theta_i - \theta_j)\ln\left(\frac{r_{i,j+1}}{r_{ij}}\right) + \cos(\theta_i - \theta_j)\beta_{ij}\right] \quad (3.36)[29]$$

Pressure coefficient is also computed from Bernoulli's equation by,

$$C_{pi} = 1 - \left(\frac{u_{ti}}{V_\infty}\right)^2 \quad (3.37)[29]$$

The coefficient of lift and pitching moment have been calculated by integrating vertical pressure acting on the surface, for different orientations of the airfoil given a constant wind velocity, to be used in optimization process.

The panel method technique presented in this chapter can estimate form drag (drag due to shape of the object) and lift-induced drag. However, it cannot be used to estimate drag due to skin friction because of the assumption that flow is inviscid (frictionless). Skin friction drag is significant at lower angles of the airfoil and therefore the panel method may not provide reliable estimates of the total drag force acting on the airfoil under those conditions. However, as the AWES being optimized in this thesis is restricted to 1D motion (altitude), friction will be negligible compared to frictional effects when crosswind motion is present. Therefore, the effects due to drag can be neglected for optimization problem considered in this thesis.

Code for flow field prediction around an airfoil using the panel method has been developed in MATLAB. The code has been designed to calculate the velocity and pressure distributions surrounding the airfoil, the lift force (coefficient of lift *Cl*), the form drag (coefficient of drag *Cd*), and the pitching moment (coefficient pf pitching moment *Cm*) acting on the airfoil. Figure 3.6 shows *Cl* values determined over a range of values of angle of attack (0-stall angle), for 3 airfoils of NACA series (-0006, -0012, -0015).

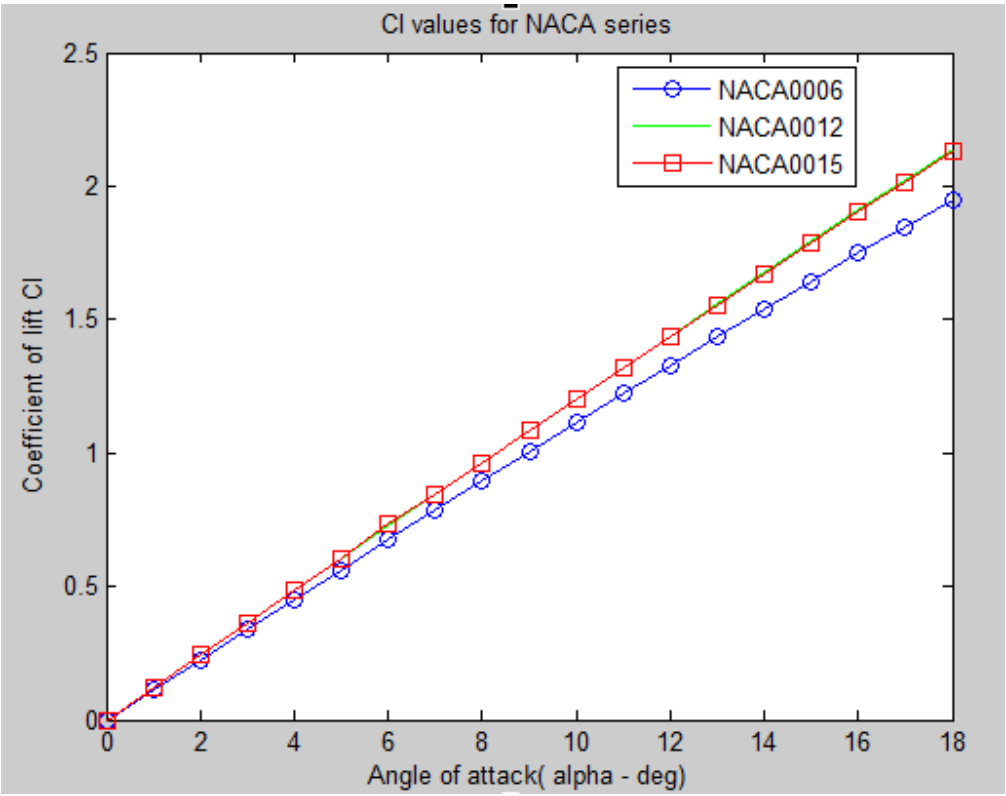

Figure **3.6**: Variation of *Cl* with geometric angle of attack α for airfoils of NACA series

The results of analysis (*Cl* values) of NACA airfoils were compared with the values extracted from the textbook Theory of Wing Sections [30] using the digitization tool *xyExtract* [31] and are found to be in close agreement. Comparison of theoretical and panel code values are shown in Figure 3.7.

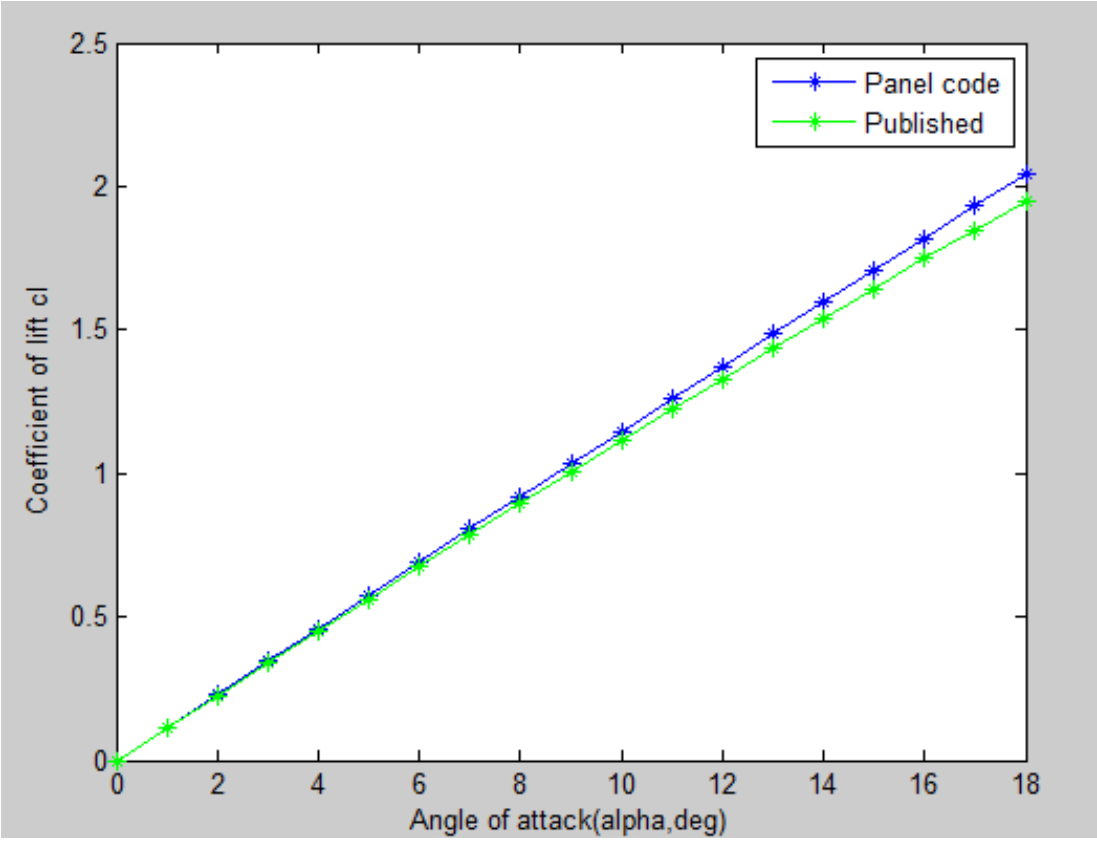

Figure **3.7**: *Cl vs α* of NACA 0012 airfoil using Panel code and Theory of Wing Sections

Variations of pitching moment and profile drag with geometric angle of attack are also shown in Figure 3.8.

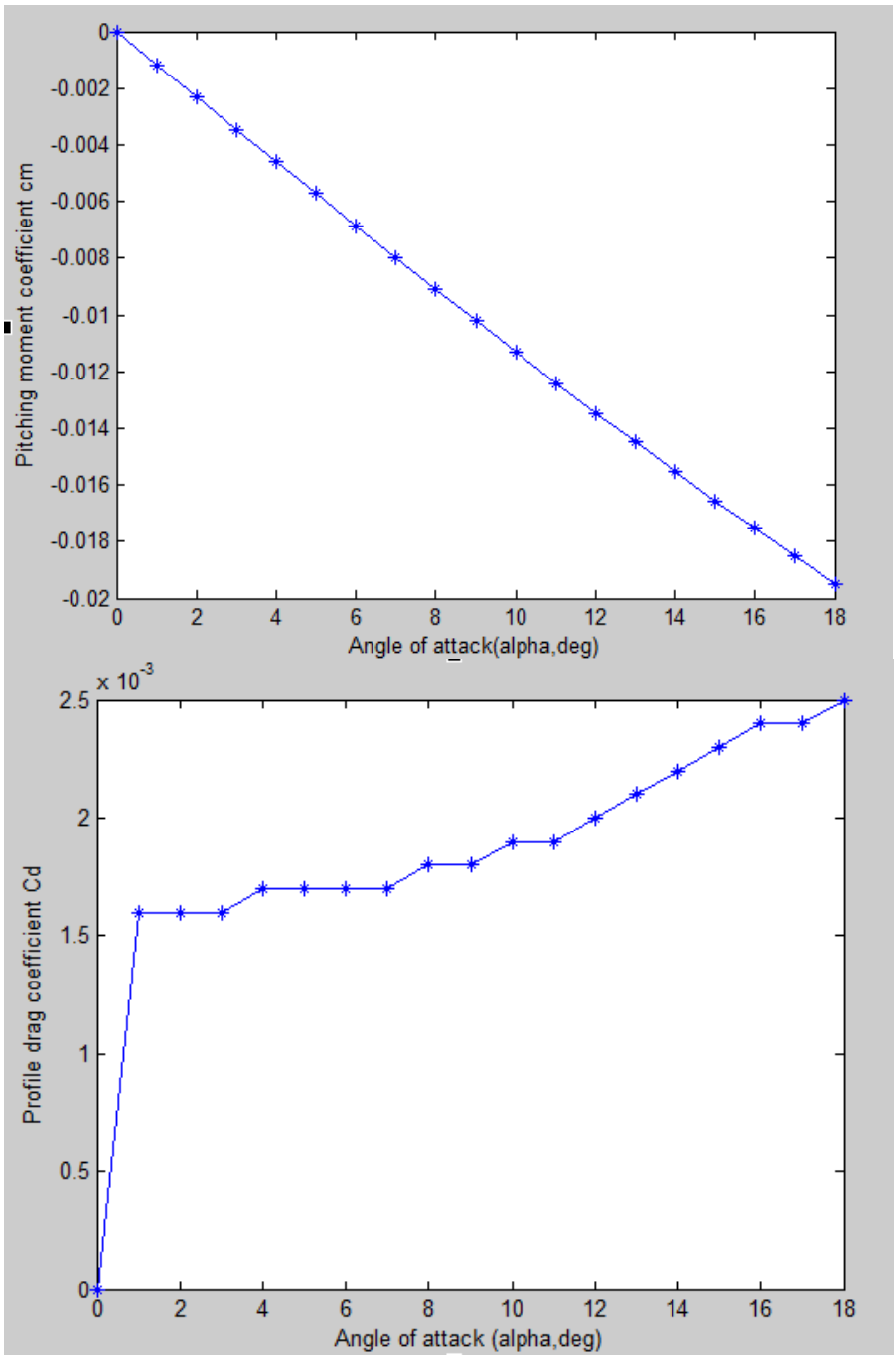

Figure **3.8**: Variation of profile drag and pitching moment coefficient with input for NACA0006.

The geometry of the NACA- 0006, 0012, 0015 airfoils have been analyzed using the code, *Cl* values for different values of angle of attack ranging from 0-18 degrees (after which the wing will stall), along with velocity and pressure distribution have been obtained. The flow field due to wind flowing at 5m/s at an angle of attack of 5^0 has been visualized in Figure 3.9, 3.10, 3.11 for three separate airfoils.

Pressure distribution over the airfoil is shown in these plots. Negative pressure observed on the upper surface of the airfoil and positive pressure seen on the lower surface of the airfoil will result in positive lift force and upward movement of the airfoil.

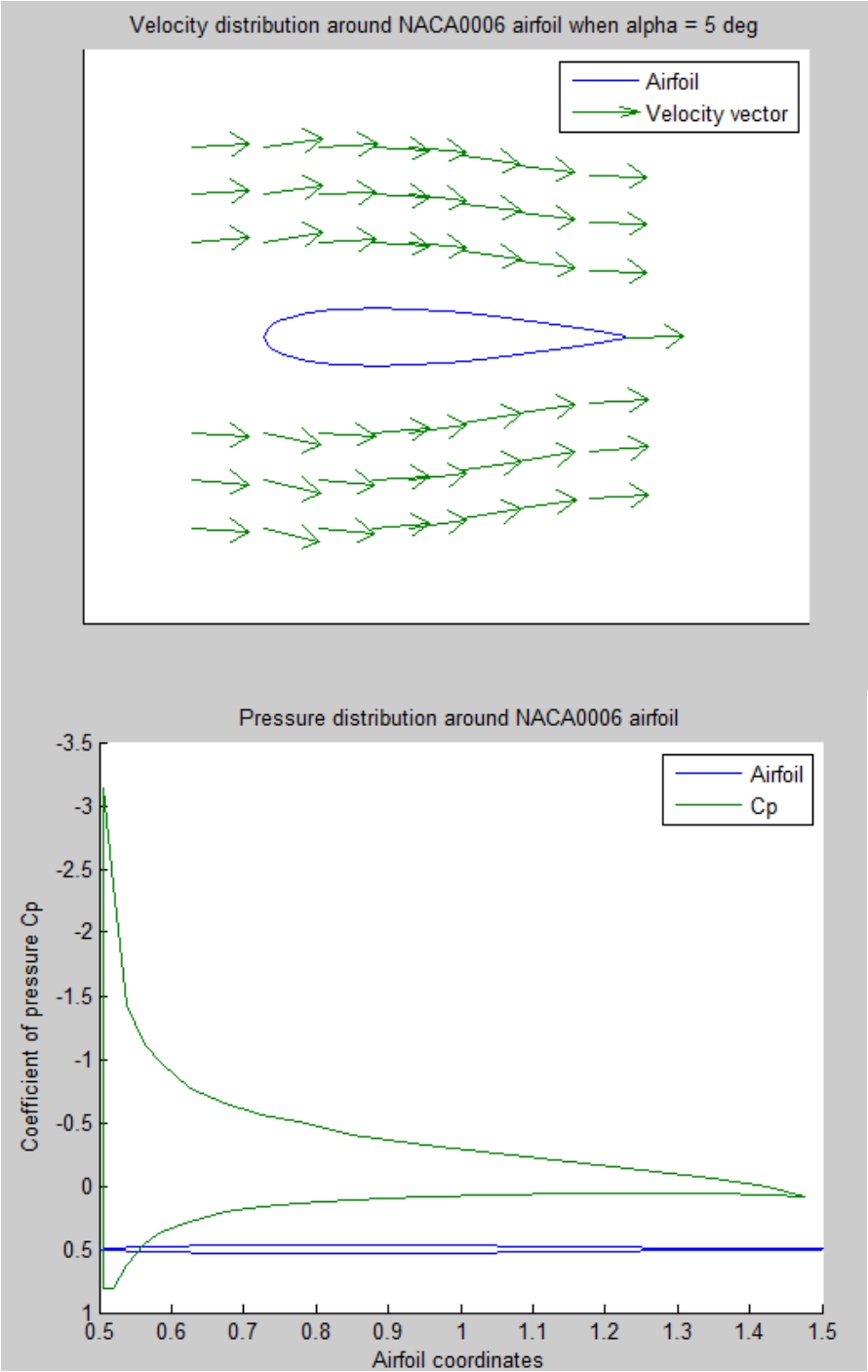

Figure **3.9**: Panel method analysis of NACA0006 airfoil

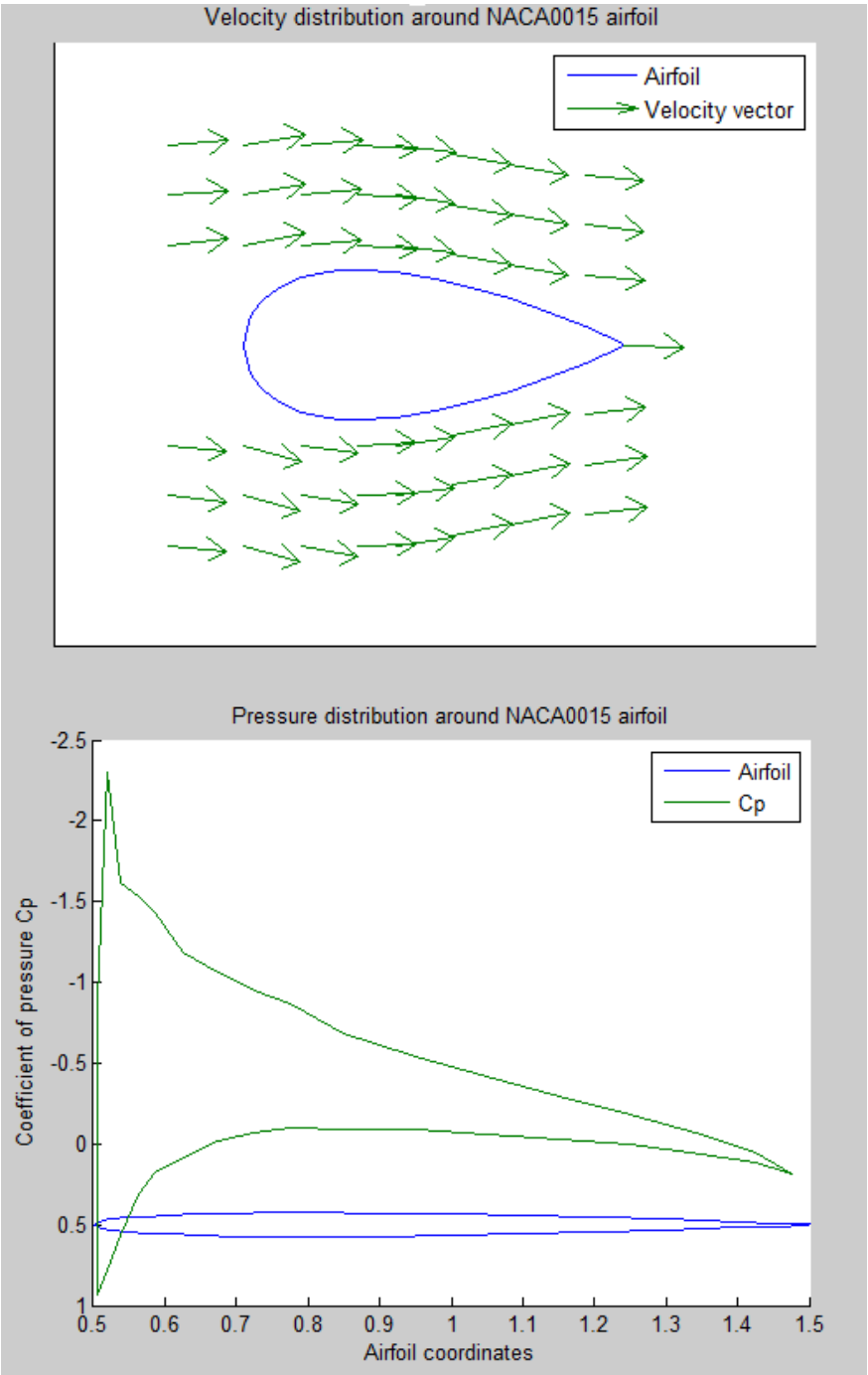

Figure **3.10**: Panel method analysis of NACA0015 airfoil.

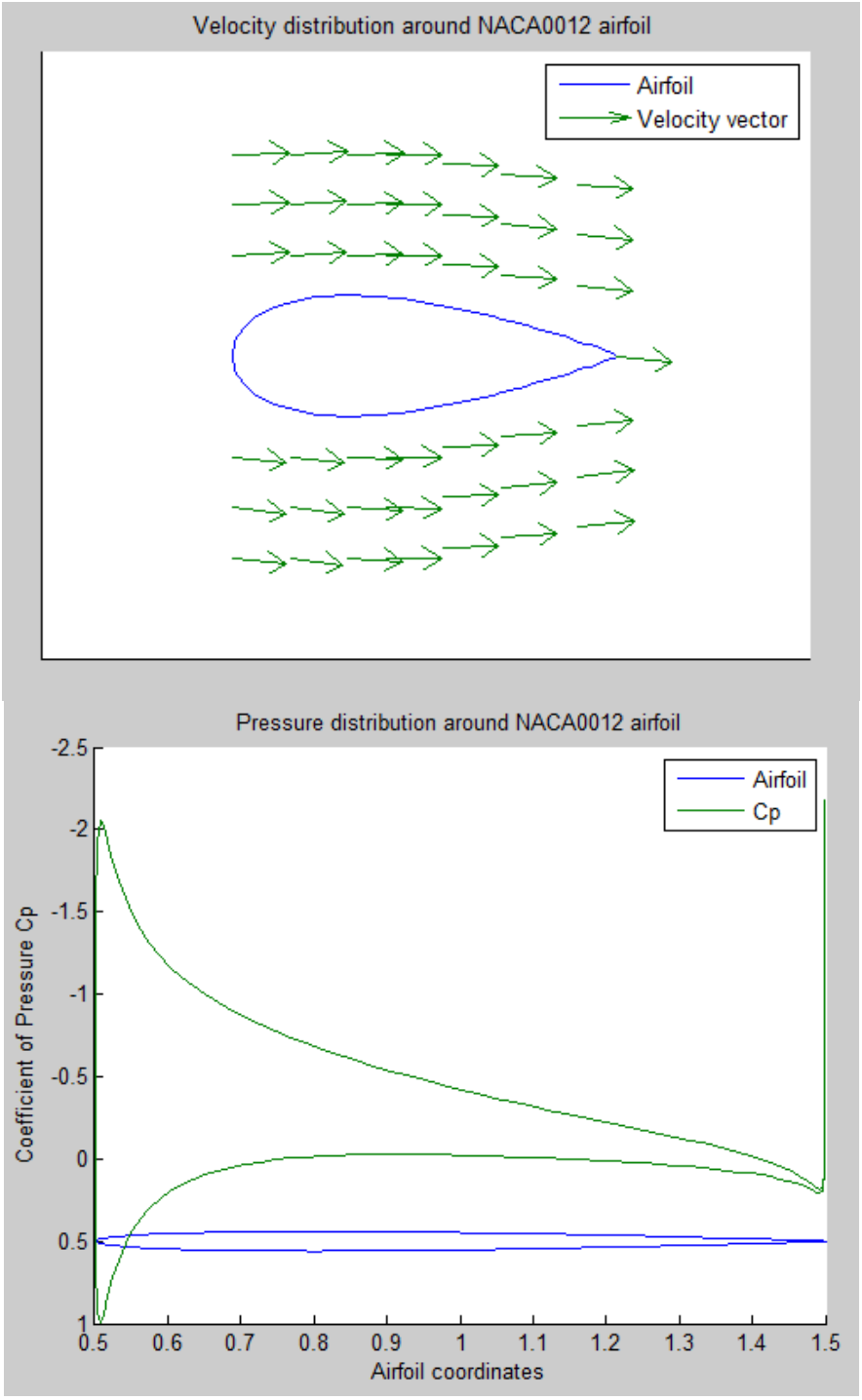

Figure **3.11**: Panel method analysis of NACA0012 airfoil

In conclusion, this chapter presents derivation of the panel method and its application in aerodynamic analysis of an airfoil shaped rotor. Validity of the results obtained have been verified and velocity and pressure distribution surrounding the airfoil have been determined. The next chapter discusses optimization of AWES using Deterministic Dynamic Programming algorithm.

Chapter 4

Optimization problem

This chapter briefly presents the optimization problem and mathematical principle behind the DDP algorithm. The dynamic models used for control in literature have varying level of complexities, depending on the control strategies explored. The airborne wind energy system is modeled as a kite or an aerostat tethered to the ground. The state space model is of the general form,

$$\dot{\overrightarrow{x(t)}} = f\left(\overrightarrow{x(t)}, \overrightarrow{u(t)}, \overrightarrow{F(t)}, \overrightarrow{W(t)}\right) \qquad (4.1)$$

where $\vec{x}$ is the vector that contains position and orientation of the rotor, $\vec{u}$ indicates linear and rotational velocities of the rotor, $\overrightarrow{W}$ indicates wind velocity and $\vec{F}$ indicates aerodynamic (and other) forces and moments acting on the airborne wind energy system.

The initial model of the dynamic system for the optimization problem is formulated by simplifying the dynamics of a general airborne wind energy system. Rotor of AWES is assumed to have geometry of NACA006 airfoil, and is of negligible mass with geometry which reduces the dynamics of the system. The rotor navigates the airspace by means of a stiff inelastic tether which can be used to adjust altitude and orientation of the rotor.

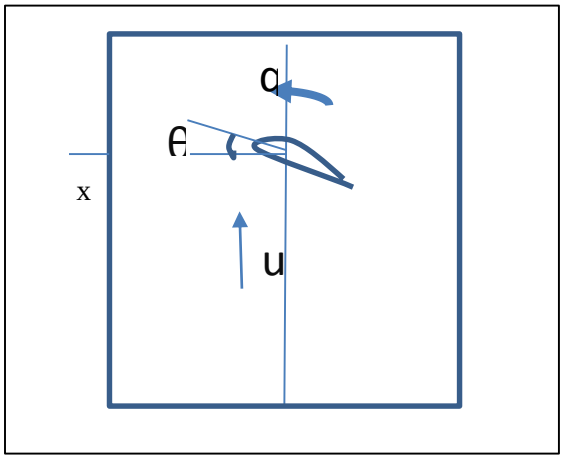

Figure 4.1: Simplified model

The optimization strategy is developed for altitude (and orientation) control of the rotor, restricting its motion to vertical direction. The position and orientation of the airfoil are taken as state variables, and rate of change of vertical position and orientation about x-axis are input variables. Under the above assumptions, the equations of dynamics will be of the form,

$$\dot{x} = u \qquad (4.2)$$

$$\dot{\theta} = q \qquad (4.3)$$

where x and θ are altitude and orientation of airfoil with respect to horizontal respectively, u and q are linear velocity and pitch (angular) velocity supplied to the airfoil by the tether.

The objective of this optimization problem is maximizing the power generated by the rotor. Since the rotor body and generator is assumed to be massless, it does not have crosswind motion and frictional effects are neglected, the main source of power generation is the lift force produced on the rotor because of its motion through wind. Instantaneous power generated at a time step is taken as a product of instantaneous lift force and imposed velocity of the airfoil. Therefore, the instantaneous objective function whose time integral is to be maximized is

$$Power\ P(u,q) = \left(\frac{1}{2} * \rho * A * vr^2 * Cl(\alpha)\right) * u \qquad (4.4)$$

where ρ, A, vr are density of air, cross-sectional area of the rotor, relative velocity of rotor with respect to wind respectively. Coefficient of lift Cl has been computed by using panel method as a function of angle of attack α in Chapter 3 and values can be seen in Figure 3.6.

4.1 Deterministic Dynamic Programming

Deterministic Dynamic programming (DDP) is a trajectory based optimization technique which solves the problems by breaking them down into incremental steps, so that optimal solutions to *sub problems* are known at any given stage and the solutions to these sub problems are then combined to solve the complete problem. DDP algorithm is guaranteed to give globally optimal solution [32, 33]. The breakdown of a problem into sub problems is based on Bellman's Principle of Optimality.

Principle of Optimality: "An optimal policy has the property that whatever the initial state and initial decision are, the remaining decisions must constitute an optimal policy with regard to the state resulting from the first decision" [32].

The DP algorithm examines the previously solved sub problems and combines their solution to give the best possible solution. The equation relating the solution of larger problem to the solutions of sub problems is called Bellman equation [33]. It writes the value of a decision at certain time as sum of value of initial choices and value of remaining decisions that results from the initial choices, i.e. it relates the objective function in one period to the objective function in the next time period. If $p(u, q)$ is the value function which gives the value associated with reaching state k from state k-1, then according to Bellman's principle of optimality,

$$P(u_k, q_k,) = \max(p(u, q) + P(u_{k-1}, q_{k-1},)) \ldots\ldots \quad (4.5)$$

where $P(x)$ is the max value associated with state $k.$, given by sum of maximum value associated with state $k-1$ and transition cost from state $k-1$ to k. In this problem, cost function $p(x)$ is given by equation for instantaneous power (4.4). Bellman equation is a necessary condition for optimality and its solution gives the result of dynamic optimization problem.

The purpose of this DDP algorithm is to compute, at every time step k, the input values that will maximize the additive objective function

$$maximize\ J = G_N + \sum_{k=1}^{n} P(u_k, q_k,) \ldots\ldots \quad (4.6)$$

Where G_N is the terminal cost at the final time step, J is the objective function $P(u_k, q_k,)$ is the transition cost at each state, which is recursive in nature and related to cost of previous state by equation (4.5)

The Dynamic Programming algorithm has been implemented by discretizing the states and inputs, splitting the duration of problem (one complete cycle of wind turbine) into several time steps. The algorithm is implemented to have same initial and terminal states (cyclic), i.e., the turbine always returns to the initial position at the end of the cycle. The value of cost function $p(u, q)$ for different values of inputs at every time step is calculated for each transition starting from terminal state at final time step to the initial state. Assuming a uniform wind profile, for each state, the inputs that give $P(u, q)$ i.e., maximum associated cost are taken as optimal inputs (solution). This comparison is repeated for all states at every time step till initial state is reached and optimal solutions to reach each state are recorded, which are then utilized to map the trajectory from initial to final state according to Bellman's Principle of Optimality.

The range of input velocities and pitch angles of -2 to 2 m/s and -2 to 2 deg/sec respectively have been found to produce reasonable relative velocities and angles of the turbine, with respect to the wind velocity of 5m/s. The effect of varying inputs to the dynamic system (u

and θ) on calculation of lift force and instantaneous power generated were plotted. Lift force acting on the airfoil will have maximum values when the airfoil is moving upwards with a positive angle of attack. The downward movement with negative angle of attack will result in the negative lift force (acting in the direction of gravity) which will most likely cause the turbine to crash. Therefore, DP algorithm has been designed to avoid this combination of inputs in computing optimal solution.

DP algorithm has iterated through the set of all possible inputs for the rotor, finding the best input for the optimum trajectory of the turbine. For each possible values of input, corresponding lift force is computed from Panel code, based on pitch angle of the turbine w.r.to relative wind velocity vector (angle of attack). Trajectories for altitude, angle of attack (relative and actual), and power produced have been generated for one periodic operation cycle of the turbine (10sec).

Turbine position is periodic as seen from Figure 4-2. Power is being generated when the airfoil is moving upwards with positive angle of attack, and positive lift force is acting on it. Power is consumed when airfoil is moving downwards. This behavior coincides with natural behavior of a wing in flight. Computing the area under the curve from Figure 4-3, it is seen that overall power generation during the flight of the turbine is positive.

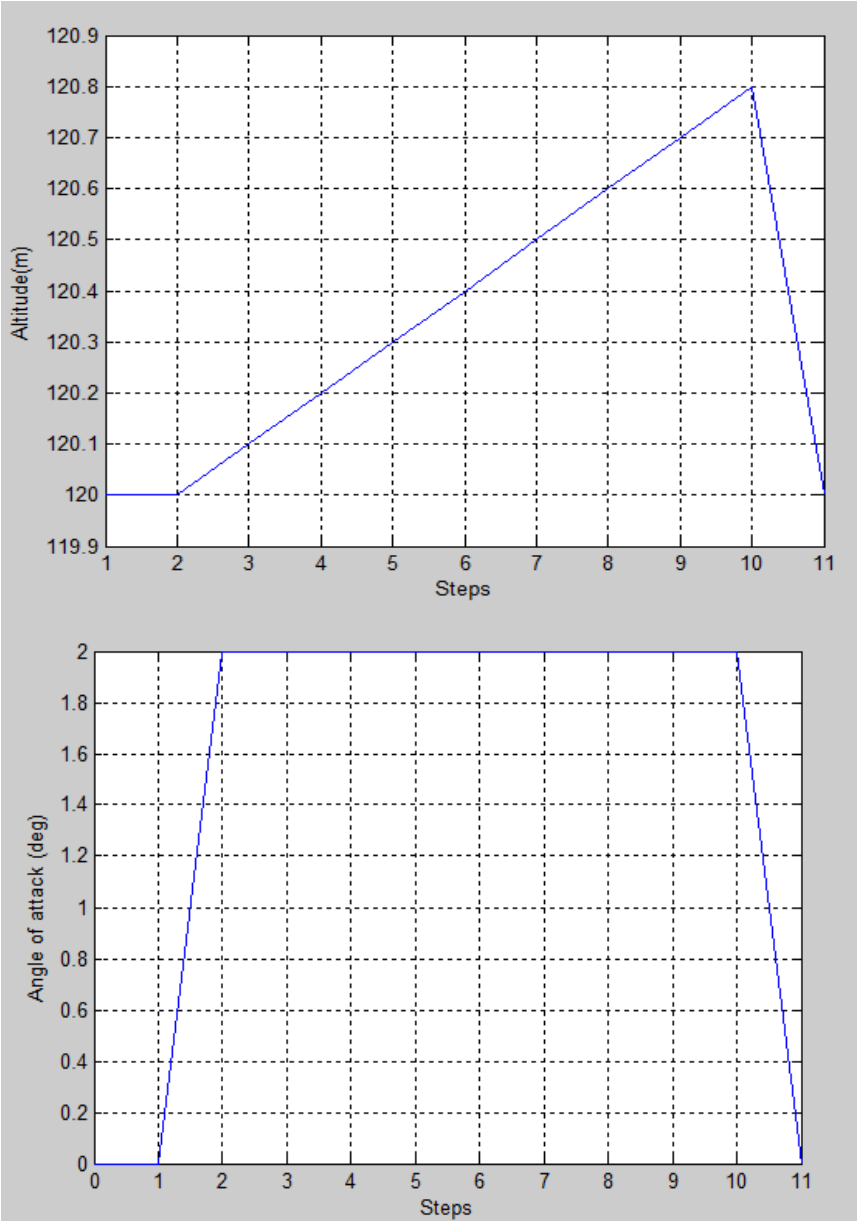

Figure 4-**2**: Profile of altitude and angle of attack during one power cycle.

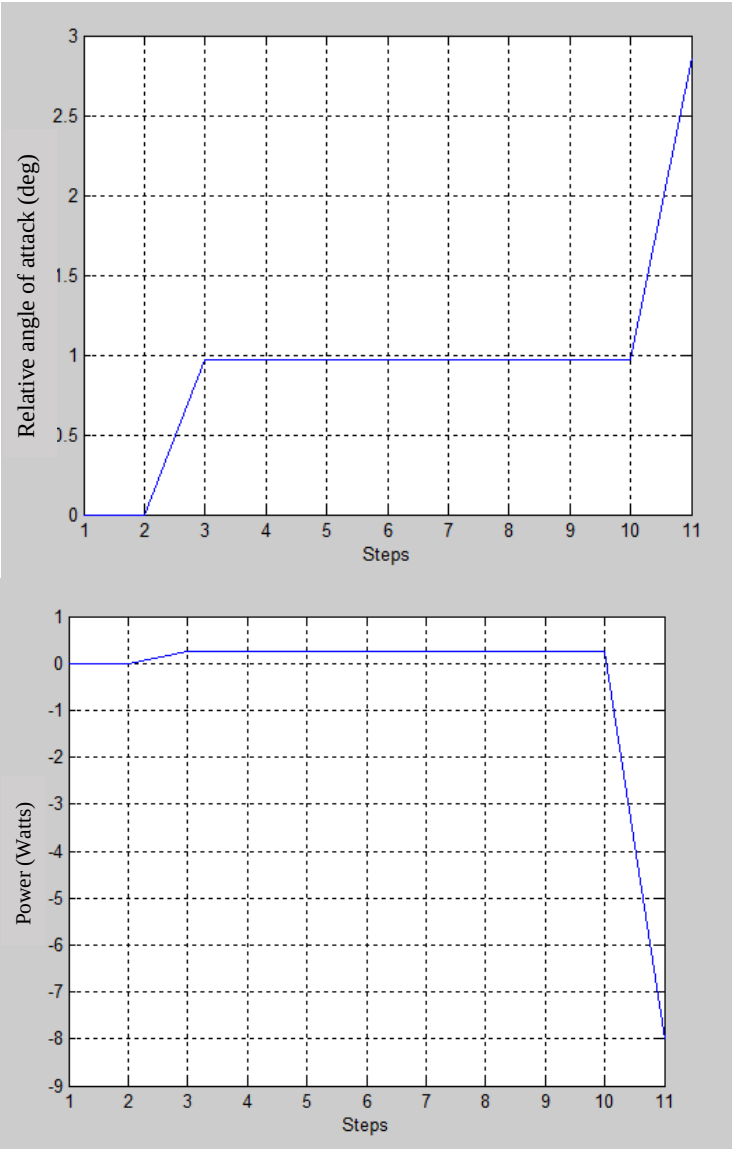

Figure **4-3**: Power production during one power cycle.

Optimal trajectory when operating the turbine for one power cycle of duration 50 sec, is shown in Figures 4-4 and 4-5. It can be observed from these plots that the trajectory shape is approximately same when the DDP algorithm is run for a longer period of time, indicating trajectory is accurate. However, more perturbations are observed in these plots compared to Figures 4-2 and 4-3.

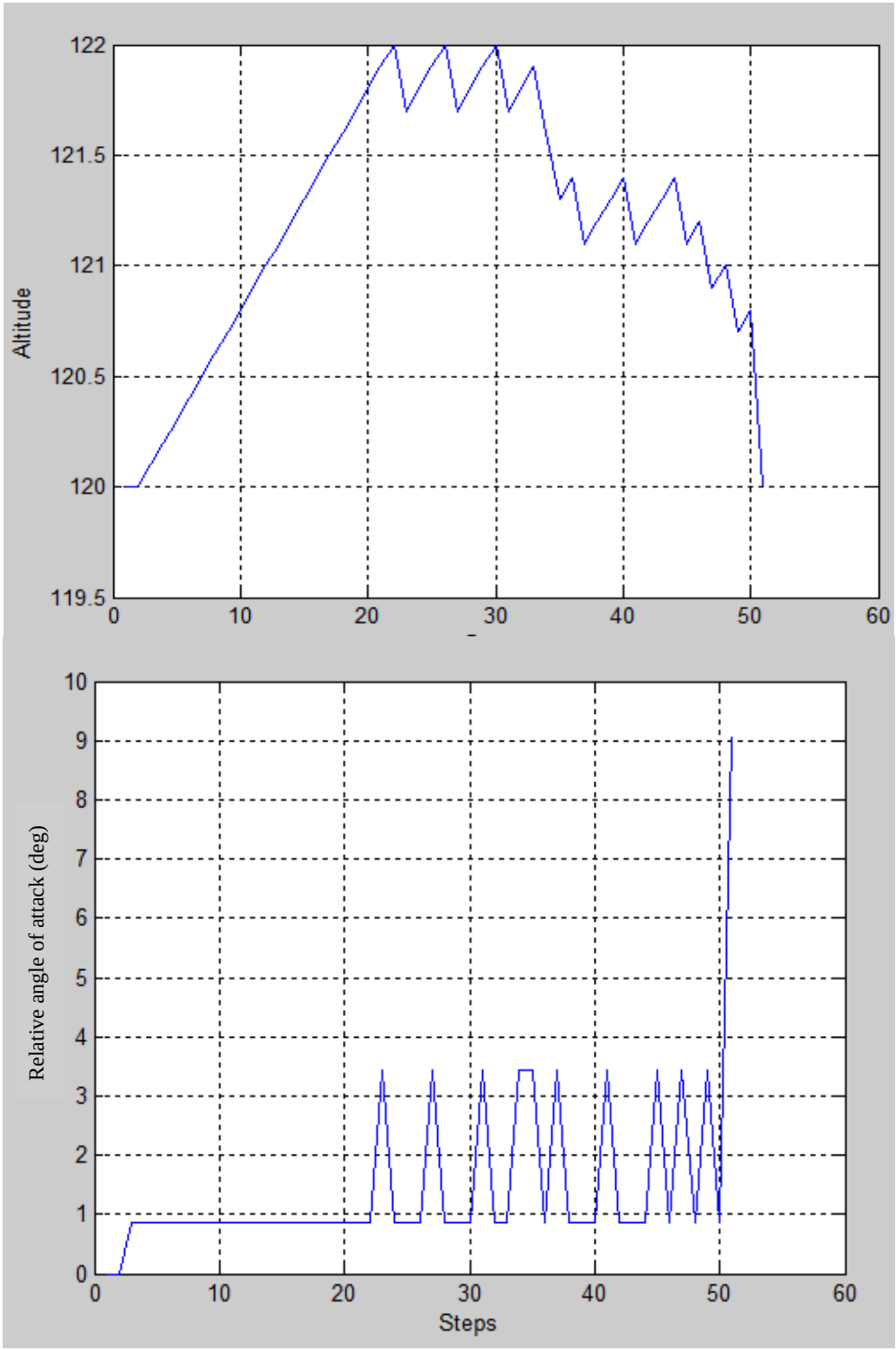

Figure **4-4**: Profile of altitude and angle of attack during one power cycle (50 sec)

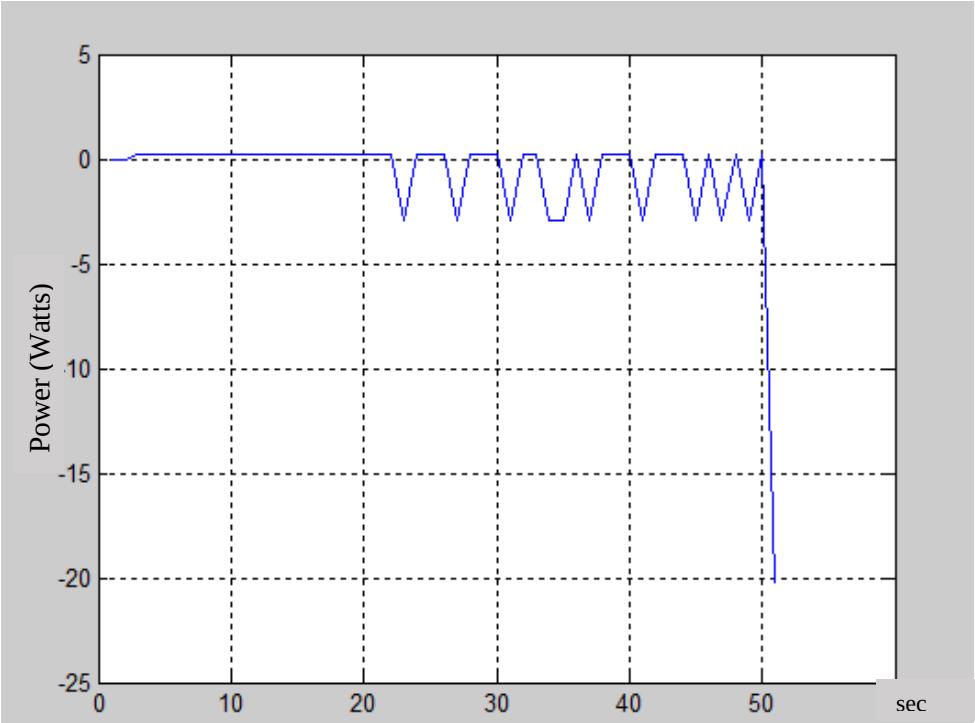

Figure **4-5**: Power production during one power cycle of duration 50 sec

To verify whether the periodic trajectory shown in Figure 4-2 is the globally optimal solution for this problem or not, the effect of mesh density on the solution is considered by computing the optimal trajectory for a range of finer input and state meshes. Mesh density has been set to the maximum, beyond which no changes in the trajectory were observed. The resultant globally optimal trajectory for maximum average power is shown in Figure 4-6, 4-7.

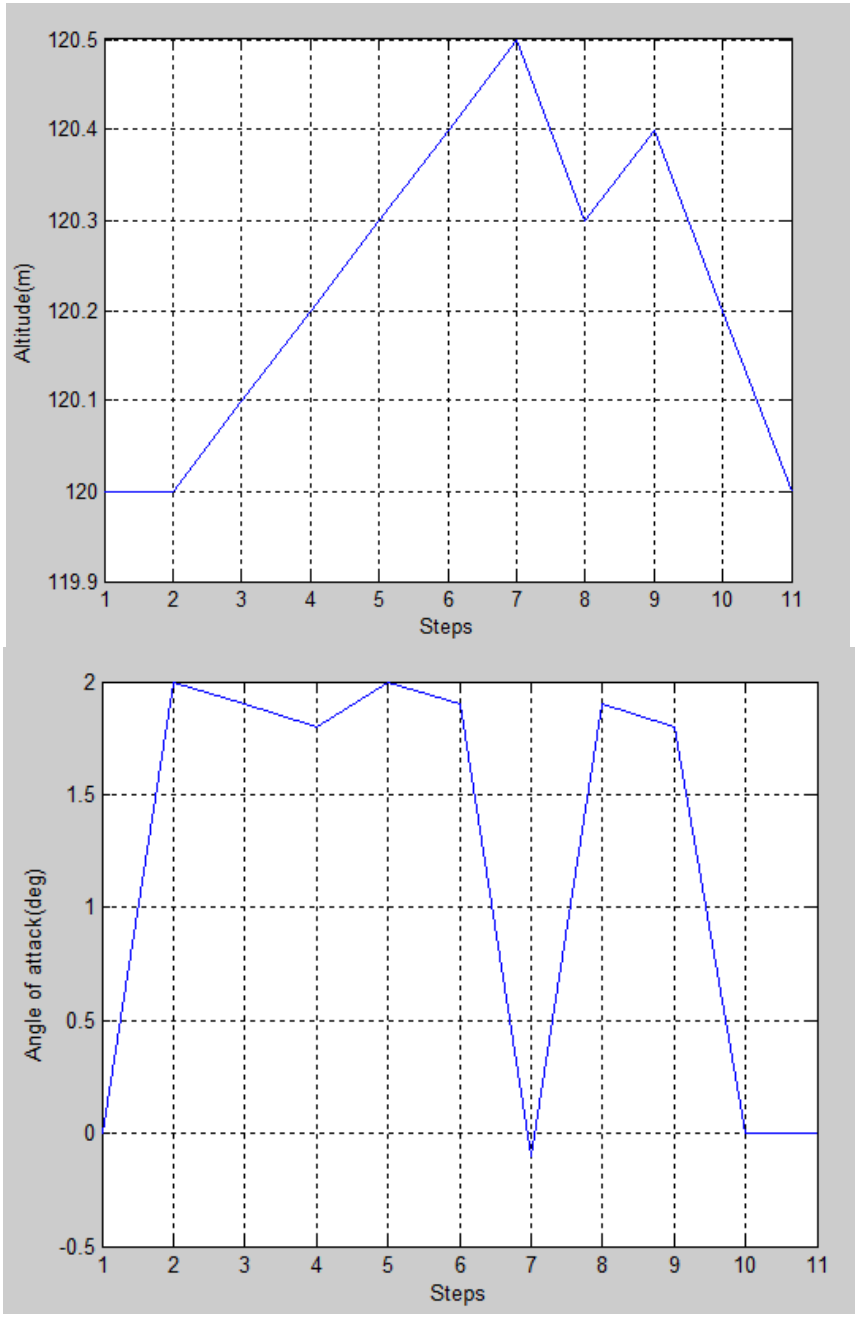

Figure **4-6**: Profile of altitude and angle of attack during one power cycle using finer mesh

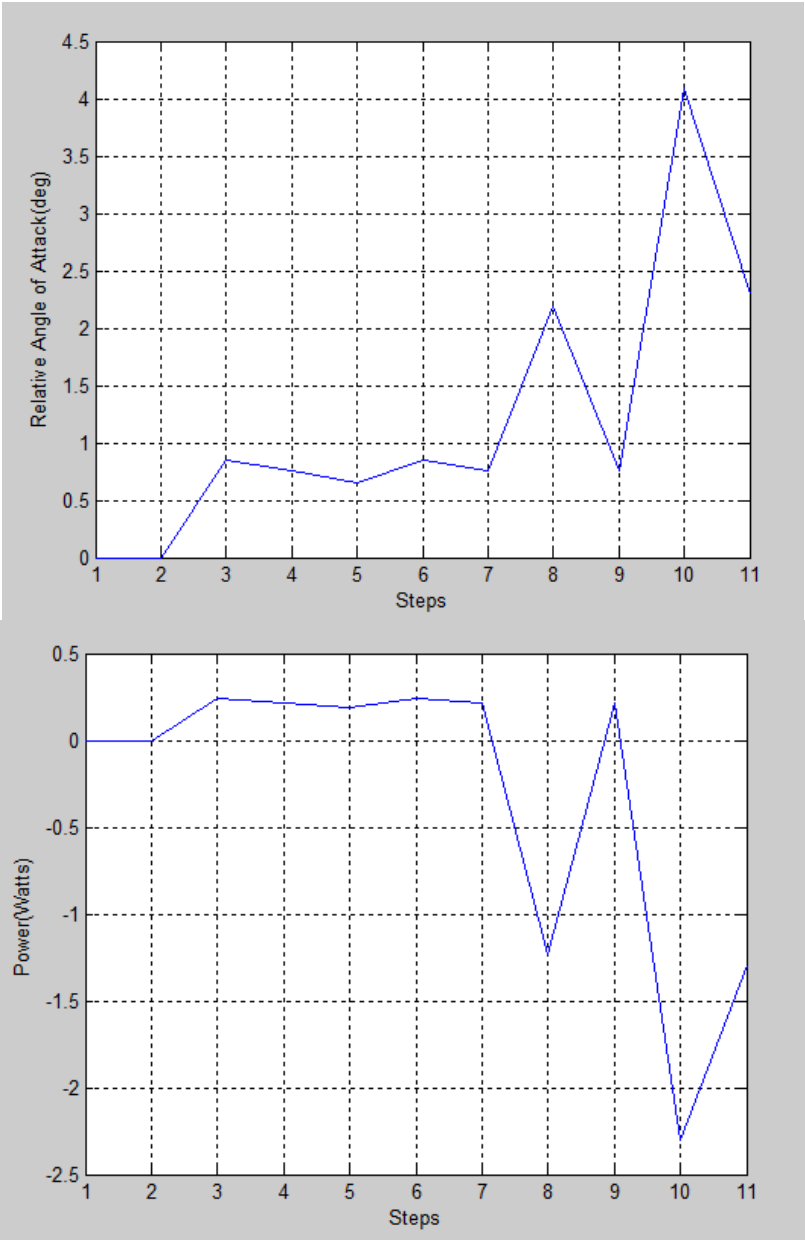

Figure **4-7**: Power production during one power cycle using finer mesh

The DDP algorithm designed above has also been applied to determine the optimal solution for maximum power generation in case of an AWES with NACA0015 airfoil rotor. The optimal trajectory and power generated have been found to be the same as in case of NACA0006 rotor (Figure 4-6, 4-7), for a fine mesh. This is because the aerodynamic characteristics (*Cl*) of

both the airfoils are approximately same (difference of order 0.01) as seen in Figure 3-6. The DDP algorithm in conjunction with panel method can be applied to rotors of varied geometries to compare their performance.

Limitations: Optimization by DDP as shown in thesis is not applicable for real-time use. The computation time and memory needed to solve the problem increases exponentially with number of independent states and inputs that need to be discretized. This is because as the problem is expanded to allow three dimensional motion for the rotor, the number of state variable involved will increase up to six, to comprehensively give out position and velocity of the airborne wind turbine. Therefore, DDP algorithm will be unwieldy when the airborne wind system is not constrained to move in one dimension. For the scope explored in this thesis, formulation of DDP algorithm is sufficient.

The accuracy of the obtained solution also depends on mesh discretization. The accuracy of the optimal trajectory obtained is directly proportional to fineness of the state and input mesh. This is because a coarse mesh is likely to result in inaccurate dynamics due to spaces in input and state grids. The DDP code has been run for different levels of discretization to observe variations in the optimal trajectory and determine globally optimal trajectory seen in Figures 4-6, 4-7. However, increasing mesh density lead to a corresponding increase in length of computation, and therefore will result in the calculation of optimal trajectory being cumbersome in the problems where mesh density needs to be increased further for an accurate optimal solution.

Chapter 5

Conclusions

5.1 Summary

As stated in Introduction, the primary goal of this project has been to develop an optimal control strategy to maximize power production in an AWT. The panel method has been used to analyze the rotor obtain velocity and pressure distribution, and lift and drag forces acting on the airfoil. The accuracy of this analysis has been verified by comparison of lift coefficient values of NACA series airfoil against those published in [29]. The basic panel method has been found to be insufficient for complete drag estimation which has considerable effect on crosswind motion. Therefore, optimal control based on these results is considered for rotor constrained to move vertically, neglecting crosswind motion. Dynamic Programming algorithm has been designed to control altitude and orientation for maximum power generation. The optimal position and orientation of turbine, for positive integral of instantaneous power generated over one operation cycle, has been identified for an AWES with airfoil shaped rotor and power overall power generated is computed.

5.2 Future work

The framework developed in this thesis by combining panel method and deterministic dynamic programming can be used for energy optimization of arbitrary shaped rotors to compare change in energy production due to change in aerodynamic characteristics. This can be used to improve shape optimization of airborne wind energy systems. Other improvements include Panel method can be extended to calculate skin friction coefficient by including temperature profiles of

the airfoil in the dynamic model used for optimization, leading to skin friction drag estimation from empirical formula to a certain known level of accuracy [29]. The DP algorithm can be further extended to include crosswind motion based on complete drag profiles from improved panel method. The effectiveness of DP algorithm can be compared to existing optimal control strategies for AWES. Other optimal control strategies might be explored as crosswind motion is included as one of the major disadvantages of DP is that increase in order of the dynamic system results in greater increase in computational complexity.

Appendix A

MATLAB CODE: Panel Method

```
%%%%%%%%%%%%%%%%%%%%%%%%%%%%%%%%%%%%%%%%%%%%%%%%%%%%%%%%%%%%%%%%%%%%%%%%%%%%%%%
%  Panel Code for aerodynamic analysis of an object in a contact with a
%  fluid
%  Written By : Ramya Cheruvu   2014.06.01
%  Aerodynamic analysis of airfoils in NACA- series
%%%%%%%%%%%%%%%%%%%%%%%%%%%%%%%%%%%%%%%%%%%%%%%%%%%%%%%%%%%%%%%%%%%%%%%%%%%%%%%


clear all
clc
clf

%  Open a File and read airfoil coordinates
load naca0012.dat
x = 0.5 + naca0012(:,1);
y = 0.5 + naca0012(:,2);


% Read Angle of Attack
alpha = 5;
pi= 3.1416;
alpha = alpha * pi /180;

n=length(x)-1;
A=zeros(n+1,n+1);
b=zeros(n+1,1);
mid=zeros(n,1);
chord = 1;
l=zeros(1,n);
cp=zeros(n,1);
q = zeros(n+1,1);

% Assembling Influence Coefficient Matrix A

for i = 1:n
   l1= x(i+1)-x(i);
   l2 = y(i+1)-y(i);
   l(i) = sqrt(l1*l1+l2*l2);%Panel length
end

for i = 1:n
 A(i,n+1) = 1.0;
```

```
 for j = 1:n
   if j ~= i
     xm1 = (x(i)+x(i+1))/2;
     ym1 = (y(i)+y(i+1))/2;
     ct  = (x(j+1)-x(j))/l(j);
     st  = (y(j+1)-y(j))/l(j);

     %collocation points to panel coordinate system
     r1  = (x(j) - xm1) * ct + (y(j) - ym1) * st;
     r2  = - (x(j) - xm1) * st +(y(j) - ym1) * ct ;
     r3  = (x(j+1) - xm1) * ct + (y(j+1) - ym1) * st;


     ys  = atan2(r2,r1)-atan2(r2,r3);
     xs  = r3 * log(r3*r3+r2*r2) - r1 * log(r1*r1+r2*r2);
     A(i,j) = (0.5 * xs-r3+r1+r2*ys)/(2*pi);%[39]
   else
     A(j,j) = l(j)*(log(l(j)/2) - 1.0)/(2*pi);%[39]
   end
 end
end

%Kutta condition
 A(n+1,1) = 1.0;
 A(n+1,n) = 1.0;

% Assemble the Right hand Side of the Matrix system
for i = 1:n
    b(i,1) = (cos(alpha) * (y(i+1)+y(i))/2) - (sin(alpha) *
(x(i+1)+x(i))/2);
end


% Solve the syetm of equations for source and vortex strength
q = A\b;

% Lift coefficient
for i = 1:n
    mid(i,1) = (x(i) + x(i+1))/2;
    cp(i,1) = 1 - q(i)^2;
    cpa = cp(i,1);
end

% Plot the airfoil
figure(1)
hold on
plot(x,y)
% Plot Cp versus airfoil coordinates
title('Pressure distribution around NACA0012 airfoil')
plot(mid,cp);
hold off
```

```
% Compute Lift and Drag Coefficients
cy = 0.0;
cx = 0.0;
cm = 0.0;
Cx = 0.0;
Cy = 0.0;
for i=1:n
    cy = - cp(i,1)*(x(i+1)-x(i));
    cx = cp(i,1)*(y(i+1)-y(i));
    Cx = Cx + cx;
    Cy = Cy + cy;
    cm = cm + cx*x(n/2) - cy*((x(i+1)+x(i))/2 - chord/4);
end

% Compute Lift and Drag coefficients

cl = Cy * cos(alpha) - Cx * sin(alpha);
cd = Cy * sin(alpha) + Cx * cos(alpha);

%%
%%%%%%%%%%%%%%%%%%%%%%%%%%%%%%%%%%%%%%%%%%%%%%%%%%%%%%%%%%%%%%%%%%%%%%%%%%%%%%%
% Flowfield prediction around the airfoil based on panel method results
%%%%%%%%%%%%%%%%%%%%%%%%%%%%%%%%%%%%%%%%%%%%%%%%%%%%%%%%%%%%%%%%%%%%%%%%%%%%%%%

ct = zeros(1,length(x)-1);
st = zeros(1,length(x)-1);
ca = cos(alpha);
sa = sin(alpha);
Vinf = 5;

% Points in airspace
V = [0.5 0.4;0.65 0.4;0.8 0.4;0.9 0.4;1.05 0.41;1.2 0.42;1.4 0.43;
     0.5 0.35;0.65 0.35;0.8 0.35;0.9 0.35;1.05 0.36;1.2 0.37;1.4 0.38;
     0.5 0.3;0.65 0.3;0.8 0.3;0.9 0.3;1.05 0.31;1.2 0.32;1.4 0.33;
     1.5 0.5;
     0.5 0.7;0.65 0.7;0.8 0.7;0.9 0.7;1.05 0.69;1.2 0.68;1.4 0.67;
     0.5 0.65;0.65 0.65;0.8 0.65;0.9 0.65;1.05 0.64;1.2 0.63;1.4 0.62;
     0.5 0.6;0.65 0.6;0.8 0.6;0.9 0.6;1.05 0.59;1.2 0.58;1.4 0.57
    ];

for i = 1:n
    ct(i) = (x(i+1)-x(i))/l(i);
    st(i) = (y(i+1)-y(i))/l(i);
end


v1 = V(:,1);
v2 = V(:,2);
n1 = numel(V)/2;
for i = 1:n1
 an(i,n+1) = 1.0 * q(n+1);
 for j = 1:n
```

```
      xm1 = v1(i);
      ym1 = v2(i);
      s1  = (x(j) - xm1) * ct(j) + (y(j) - ym1) * st(j);
      s2  = (x(j) - xm1) * st(j) +(y(j) - ym1) * ct(j) ;
      s3  = (x(j+1) - xm1) * ct(j) + (y(j+1) - ym1) * st(j);
      xs1  = (0.5)* log((s3*s3 + s2*s2)/(s1*s1 + s2*s2));
      ys1  = atan2(s2,s1)-atan2(s2,s3);
      an(i,j) = (xs1-s3+s1+s2*ys1)/(2.*pi);
      ymid = (y(j) + y(j+1))/2;
      bn(j,1) = ymid * cos(alpha) - mid(j) * sin(alpha);
      an(i,j) = an(i,j)+bn(j,1);
 end
 un(i) = sum(an(i,:));
end
for i = 1:n1
 at(i,n+1) = 0.0 * q(n+1);
 for j = 1:n
      xm1 = v1(i);
      ym1 = v2(i);
      ct  = (x(j+1)-x(j))/l(j);
      st  = (y(j+1)-y(j))/l(j);
      r1  = (x(j) - xm1) * ct + (y(j) - ym1) * st;
      r2  = - (x(j) - xm1) * st +(y(j) - ym1) * ct ;
      r3  = (x(j+1) - xm1) * ct + (y(j+1) - ym1) * st;
      xs2  = 0.5*log((r2*r2+r3*r3)/(r1*r1+r3*r3));
      ys2  = atan2(r2,r1)-atan2(r2,r3);
      at(i,j) = (0.5 * xs2-r3+r1+r2*ys2)/(2.*pi);
 end
end


ut = at*q;
for i = 1:n1
    if(v1(i)>1)
        ut(i) = -ut(i);
    end
end

% Plot the airfoil
figure(2)
hold on
plot(x,y)
%Plot the velocity field
title('Velocity distribution around NACA0012 airfoil')
quiver(v1,v2,un'/1000,ut/1000)
xlim([0 2])
ylim([0.2 0.8])
hold off
```

Bibliography

[1] C. L. Archer and M. Z. Jacobson, “Evaluation of global wind power,” J. Geophys. Res., vol. 110, 2005, D12110.

[2] R. Thresher, M. Robinson, and P. Veers, “To capture the wind,” IEEE Power Energy Mag., vol. 5, no. 6, pp. 34–46, 2007.

[3] The World Wind Energy Association (2014). 2014 Half-year Report. WWEA. pp. 1–8.

[4] M. L. Loyd, “Crosswind kite power,” J. Energy, vol. 4, no. 3,
pp. 106–111, Jul. 1980.

[5] C. Archer, K. Caldeira, “Atlas of High Altitude Wind Power,” Carnegie Institute for Science, 2008.

[7] Kitenergy Srl., http://www.kiteenergy.net.

[8] Altaeros Energies, Inc., http://www.altaerosenergies.com.

[9] Makani Power, Inc., http://makanipower.com.

[10] Ampyx Power, http:www.ampyxpower.com.

[11] SkySails GmbH and Co., http://www.skysails.info.

[12] Windlift, Inc., http://www.windlift.com.

[13] Enerkite GmbH, http://www.enerkite.com.

[14] Uwe Ahrens, Moritz Diehl, Roland Schmehl, “Airborne Wind Energy,” Springer.

[15] B. Houska and M. Diehl, “Optimal control for power generating kites,” in Proc. 9th Eur. Control Conf., Kos, Greece, 2007, pp. 3560–3567.

[16] B. Houska and M. Diehl, “Optimal control of towing kites,” IEEE conference on Decision & Control, San Diego, 2007.

[17] M. Canale, L. Fagiano, M. Milanese, and M. Ippolito, “Control of tethered airfoils for a new class of wind energy generator,” in Proc. 45th Conf. Dec. Control, 2006, pp. 4020–4026.

[18] Canale, M.; Fagiano, L.; Milanese, M.; Ippolito, M. , “KiteGen project: control as key technology for a quantum leap in wind energy generators,”American Control Conference, 2007, Page(s): 3522 – 3528

[19] P. Williams, B. Lansdorp, and W. Ockels, “Optimal cross-wind towing and power generation with tethered kites,” J. Guid. Control Dynam.,vol. 31, no. 1, pp. 81–93, 2008.

[20] Zgraggen, A.U. ; Fagiano, L. ; Morari, M. "Real-Time Optimization and Adaptation of the Crosswind Flight of Tethered Wings for Airborne Wind Energy Systems"

[21] S. Gros and M. Diehl, "A Relaxation Strategy for the Optimization of Airborne Wind Energy Systems," In European Control Conference, 2013.

[22] S. Gros, M. Zanon, and M. Diehl, "Orbit Control for a Power Generating Airfoil Based on Nonlinear MPC," In American Control Conference, 2012.

[23] Gros, S. ; Zanon, M. ; Diehl, M. , "Control of Airborne Wind Energy systems based on Nonlinear Model Predictive Control & Moving Horizon Estimation" Control Conference (ECC), 2013 European

[24] Zanon, M. ; Horn, G. ; Gros, S. ; Diehl, M. "Control of Dual-Airfoil Airborne Wind Energy systems based on nonlinear MPC and MHE" Control Conference (ECC), 2014 European

[25]L. Fagiano, A. Zgraggen, M. Morari, M. Khammash, "Automatic Crosswind Flight of Tethered Wings for Airborne Wind Energy: Modeling, Control Design, and Experimental Results," arXiv,1301.1064.2013, Submitted to IEEE Transactions on Control Systems Technology.

[26] C. Vermillion, T. Grunnagle, I. Kolmanovsky, "Modeling and Control Design for a Prototype Lighter-Than-AirWind Energy System," Proceedings of the 2012 American Control Conference, Montreal, QC.

[27] R. Weng. K. Balasubramanian, C. Vermillion, and I. Kolmanovsky, "Model predictive longitudinal control of a lighter-than-air wind energy system," in Proc. ASME Dynamic Syst. and Control Conf., Fort Lauderdale, FL, 2012.

[28] C. Vermillion, T. Grunnagle, R. Lim, I. Kolmanovsky,"Model-Based Plant Design and Hierarchical Control of a Prototype Lighter-Than-Air Wind Energy System, with Experimental Flight Test Results," Submitted (accepted) to IEEE Transactions on Control Systems Technology, 2013.

[29] Mason, "Applied Computational Aerodynamics Text"

[30] Ira H. Abbott, A.E. von Doenhoff, "Theory of Wing Sections"

[31] Wilton and Cleide Pereira da Silva, "xyExtract Graph Digitizer",

http://zeus.df.ufcg.edu.br/labfit/index_xyExtract.htm

[32] R Bellman, On the Theory of Dynamic Programming, Proceedings of the National Academy of Sciences, 1952

[33] S. Dreyfus (2002), 'Richard Bellman on the birth of dynamic programming' *Operations Research* 50 (1), pp. 48–51.

[34] S. Costello, G. François, and D. Bonvin, “Real-time optimization for kites,” in Proc. 5th Int. Fed. Autom. Control Workshop Periodic Control Syst. (IFAC-PSYCO), Caen, France, Jul. 2013, pp. 64–69.

[35] Kolar, J.W.; Friedli, T.; Krismer, F.; Looser, A.; Schweizer, M.; Steimer, P.; Bevirt, J., “Conceptualization and multi-objective optimization of the electric system of an Airborne Wind Turbine”, Industrial Electronics (ISIE), 2011 IEEE Page(s): 32-55

[36] Wen Yintang; He Junhua; Hu Zhongquan; Zhang Lili; Xu Danqin, “Design and verification of aerostat power supply system”, Control and Decision Conference (CCDC), 2013, Page(s): 2518- 2522

[37] Adhikari, J.; Rathore, A.K.; Kumar Panda, S. "Modular Interleaved Soft-Switching DC-DC Converter for High-Altitude Wind Energy Application", Emerging and Selected Topics in Power Electronics, IEEE Journal of, On page(s): 727 - 738 Volume: 2, Issue: 4, Dec. 2014

[38] Adhikari, J.; Panda, S.K. "Overview of high altitude wind energy harvesting system", Power Electronics Systems and Applications (PESA), 2013 5th International Conference on, On page(s): 1 – 8

[39] “http://soliton.ae.gatech.edu/people/lsankar/AE3903/”